Article

Molecular Cell

# Recognition of Lys48-Linked Di-ubiquitin and Deubiquitinating Activities of the SARS Coronavirus Papain-like Protease

## Graphical Abstract

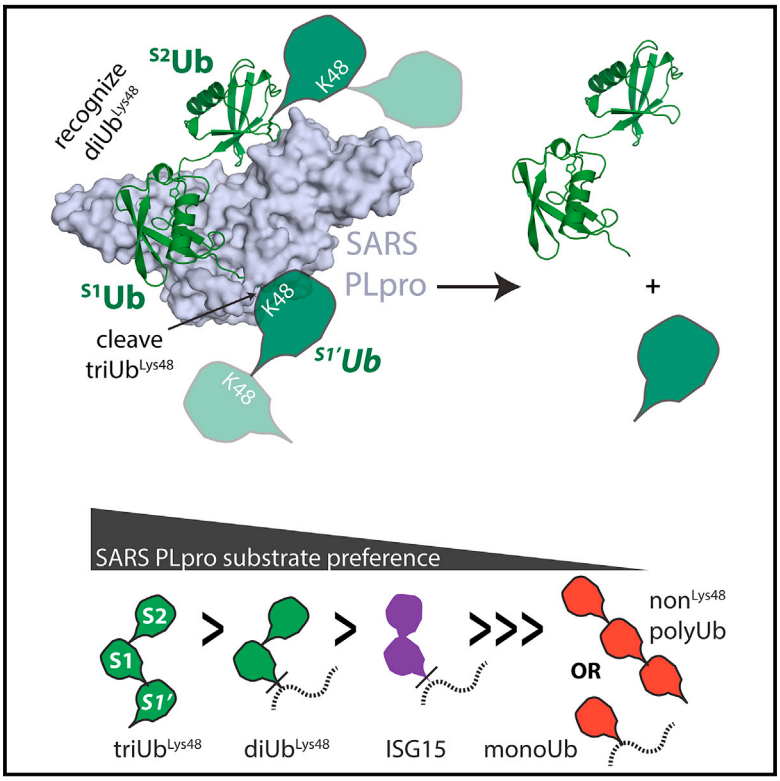


## Highlights

- A Lys48 linkage-specific diubiquitin activity-based probe selectively labels SARS PLpro
- The structure of a diUb$^{Lys48}$∼SARS PLpro complex reveals an extended di-Ub conformation
- S2-S1 and S1-S1′ interactions make SARS PLpro specific for K48-linked polyubiquitin
- SARS PLpro recognizes Lys48-linked polyUb chains and ISG15 via distinct manners

## Authors

Miklós Békés,
Gerbrand J. van der Heden van Noort,
Reggy Ekkebus, Huib Ovaa,
Tony T. Huang, Christopher D. Lima

## Correspondence

h.ovaa@nki.nl (H.O.),
tony.huang@nyumc.org (T.T.H.),
limac@mskcc.org (C.D.L.)

## In Brief

Békés et al. present a high-resolution crystal structure of a SARS virus PLpro∼diUb$^{Lys48}$ complex that reveals an extended conformation of the Lys48-linked diUb unit and shows the biochemical basis for SARS PLpro's preference for Lys48-linked polyUb chains.

## Accession Numbers

5E6J

Békés et al., 2016, Molecular Cell 62, 572–585
May 19, 2016 
http://dx.doi.org/10.1016/j.molcel.2016.04.016

CellPress

Molecular Cell
Article

# Recognition of Lys48-Linked Di-ubiquitin and Deubiquitinating Activities of the SARS Coronavirus Papain-like Protease

Miklós Békés,[1,2] Gerbrand J. van der Heden van Noort,[4] Reggy Ekkebus,[4] Huib Ovaa,[4,5,*] Tony T. Huang,[1,5,*] and Christopher D. Lima[2,3,5,*]

[1]Department of Biochemistry and Molecular Pharmacology, New York University School of Medicine, New York, NY 10016, USA
[2]Structural Biology Program, Sloan Kettering Institute, 1275 York Avenue, New York, NY 10065, USA
[3]Howard Hughes Medical Institute, 1275 York Avenue, New York, NY 10065, USA
[4]Division of Cell Biology II, The Netherlands Cancer Institute (NKI), Plesmanlaan 121, 1066 CX Amsterdam, the Netherlands
[5]Co-senior author
*Correspondence: h.ovaa@nki.nl (H.O.), tony.huang@nyumc.org (T.T.H.), limac@mskcc.org (C.D.L.)
http://dx.doi.org/10.1016/j.molcel.2016.04.016

## SUMMARY

**Deubiquitinating enzymes (DUBs) recognize and cleave linkage-specific polyubiquitin (polyUb) chains, but mechanisms underlying specificity remain elusive in many cases. The severe acute respiratory syndrome (SARS) coronavirus papain-like protease (PLpro) is a DUB that cleaves ISG15, a two-domain Ub-like protein, and Lys48-linked polyUb chains, releasing diUb$^{Lys48}$ products. To elucidate this specificity, we report the 2.85 Å crystal structure of SARS PLpro bound to a diUb$^{Lys48}$ activity-based probe. SARS PLpro binds diUb$^{Lys48}$ in an extended conformation via two contact sites, S1 and S2, which are proximal and distal to the active site, respectively. We show that specificity for polyUb$^{Lys48}$ chains is predicated on contacts in the S2 site and enhanced by an S1-S1′ preference for a Lys48 linkage across the active site. In contrast, ISG15 specificity is dominated by contacts in the S1 site. Determinants revealed for polyUb$^{Lys48}$ specificity should prove useful in understanding PLpro deubiquitinating activities in coronavirus infections.**

## INTRODUCTION

Viruses can dampen the host anti-viral response by hijacking the ubiquitin (Ub) system (Bhoj and Chen, 2009; Isaacson and Ploegh, 2009) by expressing factors such as viral deubiquitinating enzymes (DUBs) that antagonize Ub-dependent pro-inflammatory pathways (Bailey-Elkin et al., 2014b; Capodagli et al., 2011; Mielech et al., 2014). For instance, the severe acute respiratory syndrome (SARS) and Middle East respiratory syndrome (MERS) human coronaviruses encode viral polypeptide processing proteases that can also catalyze deubiquitinating and deISGylating activities. The relevant host substrates of these viral DUBs and their mechanisms of target selection remain poorly defined.

Ub-dependent signaling pathways are regulated by the type of Ub modification (mono-ubiquitin [monoUb] or polyubiquitin [polyUb]) or type of Ub chain linkage utilized (Pickart, 2001), as polyUb chains can be formed by conjugation to any of Ub's seven lysine (Lys) residues or its N-terminal methionine (Komander and Rape, 2012). DUB-mediated cleavage of Ub chains or conjugates serves as a critical regulator or antagonist of Ub-driven signaling pathways (Reyes-Turcu et al., 2009).

While the molecular basis for monoUb specificity for many human and viral DUBs was revealed in structures of monoUb-bound DUB complexes, the molecular basis of Ub chain linkage specificity is understood only for a handful of DUBs (Keusekotten et al., 2013; Mevissen et al., 2013; Sato et al., 2015). In these cases, specificity is dictated by direct readout of a particular isopeptide-linkage via binding the primed (S1′) Ub and unprimed, or proximal, (S1) Ub across the DUB active site. In one case, Lys11-specificity of the OTUD2 catalytic core is achieved by recognizing S1′ Ub and S1 Ub across the DUB active site, an activity that is aided by another domain that contacts a third Ub in a distal S2 site (Mevissen et al., 2013). Lys48-linked Ub chains are highly abundant in cells (Kirkpatrick et al., 2006), and their conjugation to other proteins targets them for proteasomal degradation (Chau et al., 1989), but the molecular basis for DUB recognition of Lys48-linked Ub chains remains unclear.

Ub-based chemical probes have been widely used to profile DUB activities and to stabilize monoUb-bound DUB complexes for structure determination (Ekkebus et al., 2013; Hemelaar et al., 2004). Total chemical synthesis of di-ubiquitin (diUb) activity-based probes (Ub-ABPs), with Cys-reactive warheads at the isopeptide linkage of choice (Mulder et al., 2014) enabled profiling of DUB linkage-specificities across S1-S1′; however these ABPs are not suitable for characterizing DUBs that recognize Ub chain topology through alternative mechanisms.

We and others recently showed that a coronavirus DUB, SARS papain-like protease (PLpro), but not MERS PLpro, preferentially recognizes and releases diUb$^{Lys48}$ units during cleavage of polyUb chains by an alternative mechanism that relies on SARS PLpro recognition of diUb via at least two binding sites

in S2-S1, rather than S1-S1′ (Békés et al., 2015; Ratia et al., 2014). The structure of SARS PLpro bound to monoUb revealed surfaces required for S1 recognition and plausible explanations for Ub chain specificity and potential surfaces important for S2 recognition (Ratia et al., 2014), but the molecular basis for SARS PLpro Lys48-Ub chain specificity remains unknown. We report the crystal structure of SARS PLpro bound to a diUb$^{Lys48}$-ABP. The structure reveals SARS PLpro DUB recognition of an extended Lys48-linked diUb chain via distinct $^{S1}$Ub and $^{S2}$Ub binding sites, and biochemical studies show that $^{S2}$Ub binding is most important for polyUb processing. The molecular basis for diUb$^{Lys48}$ recognition by a Lys48-specific DUB has remained unclear, and in this case, SARS PLpro Ub chain specificity is dominated by indirect readout of a unique diUb chain conformation at a site distal from the active site.

## RESULTS

### A DiUb$^{Lys48}$ Activity-Based Probe Preferentially Labels SARS PLpro

SARS PLpro and MERS PLpro are efficient deubiquitinating enzymes, on par with other human DUBs (Báez-Santos et al., 2014; Békés et al., 2015; Ratia et al., 2014); however, SARS PLpro rapidly removes Lys48-linked Ub chains from conjugated substrates, including polyubiquitinated IκBα stabilized by tumor necrosis factor α (TNF-α)/MG132 treatment (Figure 1A), and is unique in its recognition and release of diUb$^{Lys48}$ units from chains of three or more Ubs (Békés et al., 2015). This unique activity is striking when compared to the related MERS PLpro, since they are structurally similar and share 52% amino acid sequence homology (Báez-Santos et al., 2014). While SARS PLpro efficiently cleaves higher-molecular-weight (HMW) polyUb$^{Lys48}$ conjugates, it exhibits poor activity in cleavage assays using free diUb chains or mono- or di-ubiquitinated substrates, such as IκBα (Figure 1A). These data supported a model whereby SARS PLpro uses distal Ub binding site (S2) to recognize diUb$^{Lys48}$ across S2-S1 (Figure 1B), rather than across S1-S1′, as is typical for most DUBs.

To provide evidence for this model, a singly N-terminal biotin-tagged triUb$^{Lys48}$ chain (Figure 1C) was generated (Figures S1A–S1G) and cleaved using SARS PLpro. Analysis of cleavage intermediates shows that the N-terminal biotin-label is retained on the diUb product (Figure 1D, right), suggesting that tri-ubiquitin (triUb) recognition requires binding via S2-S1, in a distal-to-proximal direction (Figure 1C, top schematics). In contrast, cleavage intermediates produced by other USP-family DUBs contain mixtures of mono- and diUb products bearing the biotin tag (Figure S2A). USP21$_{CD}$ and USP2$_{CD}$ show little preference, while MERS PLpro displays a slight preference.

We next took advantage of linkage-specific diUb activity-based probes that place warheads at the isopeptide linkage (Figure 1E, "in-between"; Mulder et al., 2014) or proximal end (Figure 1E, "distal diUb$^{Lys48}$," green, right cartoon; Flierman et al., 2016). The distal diUb-ABP bears an isosteric non-hydrolyzable triazole linker in lieu of the native isopeptide linkage (Figure S2B). In labeling assays with SARS PLpro (Figure 1E), the distal diUb$^{Lys48}$-ABP (green) reacted well, monoUb-ABP (orange) reacted slowly, and the in-between diUb$^{Lys48}$-ABP (red) reacted poorly, and quantification shows distal diUb$^{Lys48}$-ABP adduct forms most efficiently in comparison to other probes (Figures 1F and S2C). The observation that SARS PLpro formed adducts least efficiently with the in-between diUb$^{Lys48}$-ABP probe (compare to monoUb-ABP), suggests that it might bind the in-between diUb$^{Lys48}$-ABP via S2-S1, preventing it from binding and reacting via S1-S1′ interactions (Figure S2D). Importantly, the in-between diUb$^{Lys48}$-ABP efficiently labels other DUBs that do not exhibit diUb preferences (Figures S2E and S2F). With the ideal reagent in hand, we set out to determine the structural basis for diUb$^{Lys48}$ recognition by SARS PLpro.

### Crystal Structure of SARS PLpro Bound to a DiUb$^{Lys48}$-ABP

SARS PLpro was cross-linked to the distal diUb$^{Lys48}$-ABP, purified and crystallized. Crystals diffracted to 2.85 Å, and a structure of SARS PLpro-diUb$^{Lys48}$-ABP (Figure 2A) was determined by molecular replacement (Supplemental Experimental Procedures). Two SARS PLpro-diUb$^{Lys48}$-ABP complexes occupy the asymmetric unit. The model was refined to an $R_{work}/R_{free}$ of 23.2/26.4 with good stereochemistry (Table 1). One of the two complexes exhibits continuous electron density, while the other is less ordered with some discontinuity. Electron density is evident for the propargyl warhead of diUb$^{Lys48}$-ABP and active site Cys112 of SARS PLpro in both complexes (Figure S3A), but the diUb Lys48 isopeptide-mimic triazole linkage is weaker in one complex (Figure S3B).

The diUb$^{Lys48}$-ABP-bound SARS PLpro structure reveals the basis for SARS PLpro catalytic domain recognition of proximal ($^{S1}$Ub) and distal ($^{S2}$Ub) Ub molecules within the context of a diUb$^{Lys48}$ unit. The SARS PLpro catalytic domain includes an N-terminal Ub-like (Ubl) domain that is dispensable for SARS PLpro activity (Békés et al., 2015; Mielech et al., 2014), followed by classical palm and finger DUB domains, as described for SARS PLpro (Ratia et al., 2006) and other USP-family member DUBs (Reyes-Turcu et al., 2009). The DUB catalytic module superposes well between diUb$^{Lys48}$-ABP-bound SARS PLpro and structures of apo (PDB: 2FE8) or monoUb-bound SARS PLpro (PDB: 4MM3; Figures S3C and S3D), with root-mean-square deviation (rmsd) values of 0.56 Å and 0.44 Å over 255 amino acids (Ser61-Ile315), respectively.

The orientation of diUb$^{Lys48}$ bound to SARS PLpro is different from prior structures of Lys48-linked Ub chains, whether bound or unbound; this is most apparent when our structure is compared to the "closed" conformation of diUb$^{Lys48}$ (PDB: 1AAR; Cook et al., 1992; Figure 2B). It appears that SARS PLpro stabilizes Lys48-linked Ub chains in an extended conformation, akin to conformations of Lys63- or Met1-linked diUb (Komander et al., 2009), yet distinct from those as well. Although SARS PLpro contacts $^{S2}$Ub and $^{S1}$Ub, it makes few contacts to the interface between $^{S2}$Ub and $^{S1}$Ub or the isopeptide analog (Figure 2C).

The position of $^{S1}$Ub within SARS PLpro-diUb$^{Lys48}$-ABP is similar to the monoUb-SARS PLpro structure (Ratia et al., 2014), including contacts to the $^{S1}$Ub C terminus; the $^{S1}$Ub-Ile44 patch via Met209 of SARS, and polar contacts to $^{S1}$Ub-Gln49 and $^{S1}$Ub-Arg42 by the SARS PLpro palm domain via Arg167 and Asp168, respectively (Figure 2D). The related viral

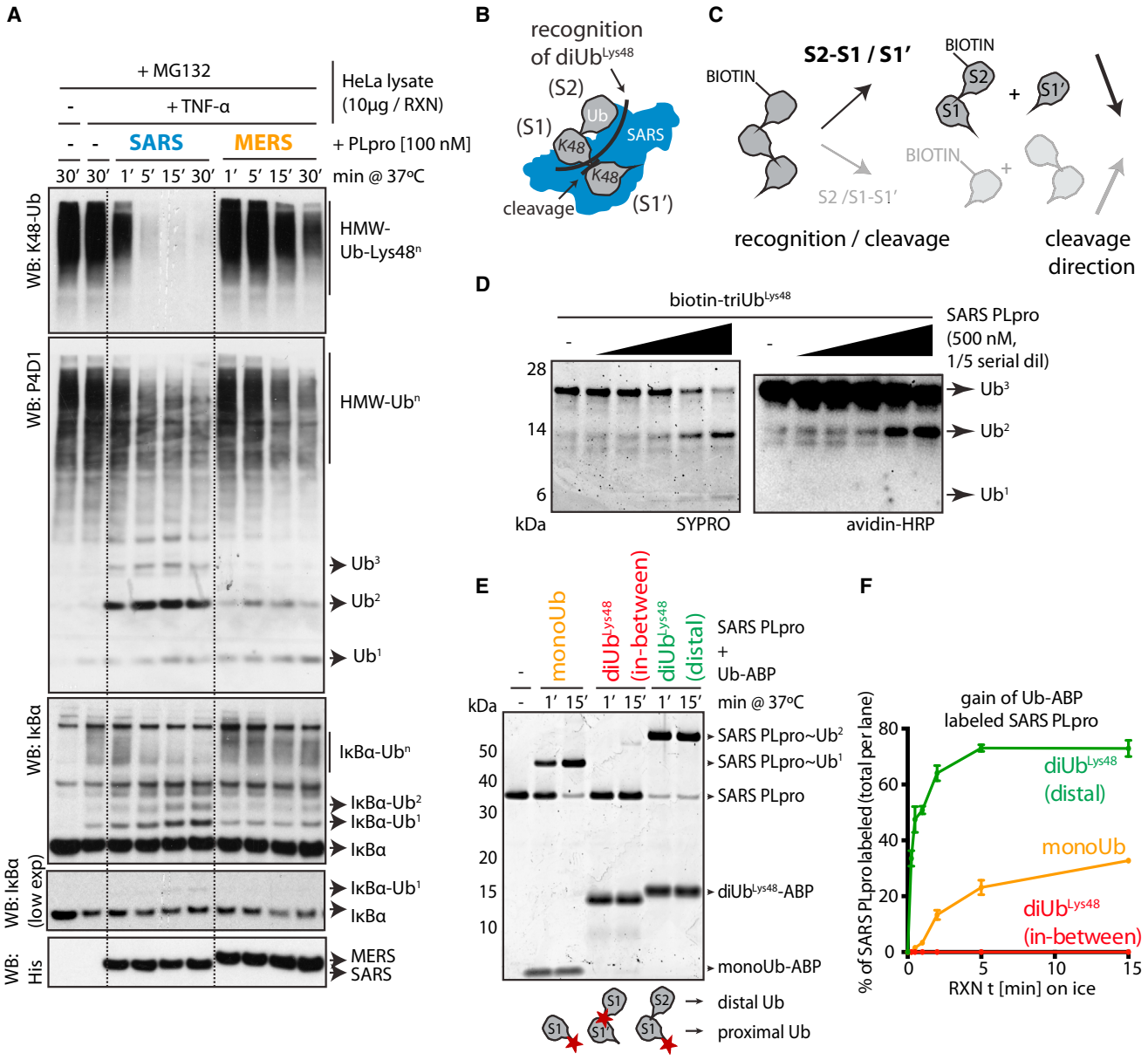


**Figure 1. Distal diUb$^{Lys48}$ ABP Labels SARS PLpro**

(A) Ub-conjugate cleavage in TNF-α-treated HeLa cell lysates by SARS and MERS PLpro. Dotted lines added for clarity.

(B and C) Schematics of (B) Ub chain recognition by SARS PLpro and (C) recognition and cleavage of biotin-tagged triUb$^{Lys48}$.

(D) Cleavage of biotin-triUb$^{Lys48}$ by SARS PLpro. Cleavage intermediates detected by avidin-HRP reveal biotin on the diUb product.

(E) Qualitative labeling of SARS PLpro by Ub-ABPs (cartoons at bottom with red stars indicate warhead positions).

(F) Quantitative labeling of SARS PLpro by Ub-ABPs indicating percent of SARS PLpro labeled as derived from gels in Figure S2C. Error bars represent ±SEM.

See also Figures S1 and S2.

DUB, MERS PLpro, recognizes $^{S1}$Ub in a similar manner, yet specific contacts to the $^{S1}$Ub-Ile44 patch are not identical (Bailey-Elkin et al., 2014a). Additionally, SARS PLpro cradles $^{S1}$Ub with its fingers domain, with $^{S1}$Ub interaction surfaces comprising the largest buried interaction surface area (~890 Å$^2$). In comparison to apo SARS, both structures with monoUb and diUb bound reveal similar displacements of the BL2-loop (Figure S3E) that accommodates the Ub C-terminal tail in the active site (Ratia et al., 2014). When compared to the monoUb-bound SARS PLpro complex, a small conformational change is observed in $^{S1}$Ub with respect to displacement of a loop between Ub amino acids 51–57 that is next to Lys48 and the triazole linkage (Figures S3F and S3G). To query if displacement could be due to the triazole linkage, our diUb structure was compared to Lys48-linked diUb (PDB 1AAR) revealing that amino acids 51–57 adopt a similar conformation to that observed

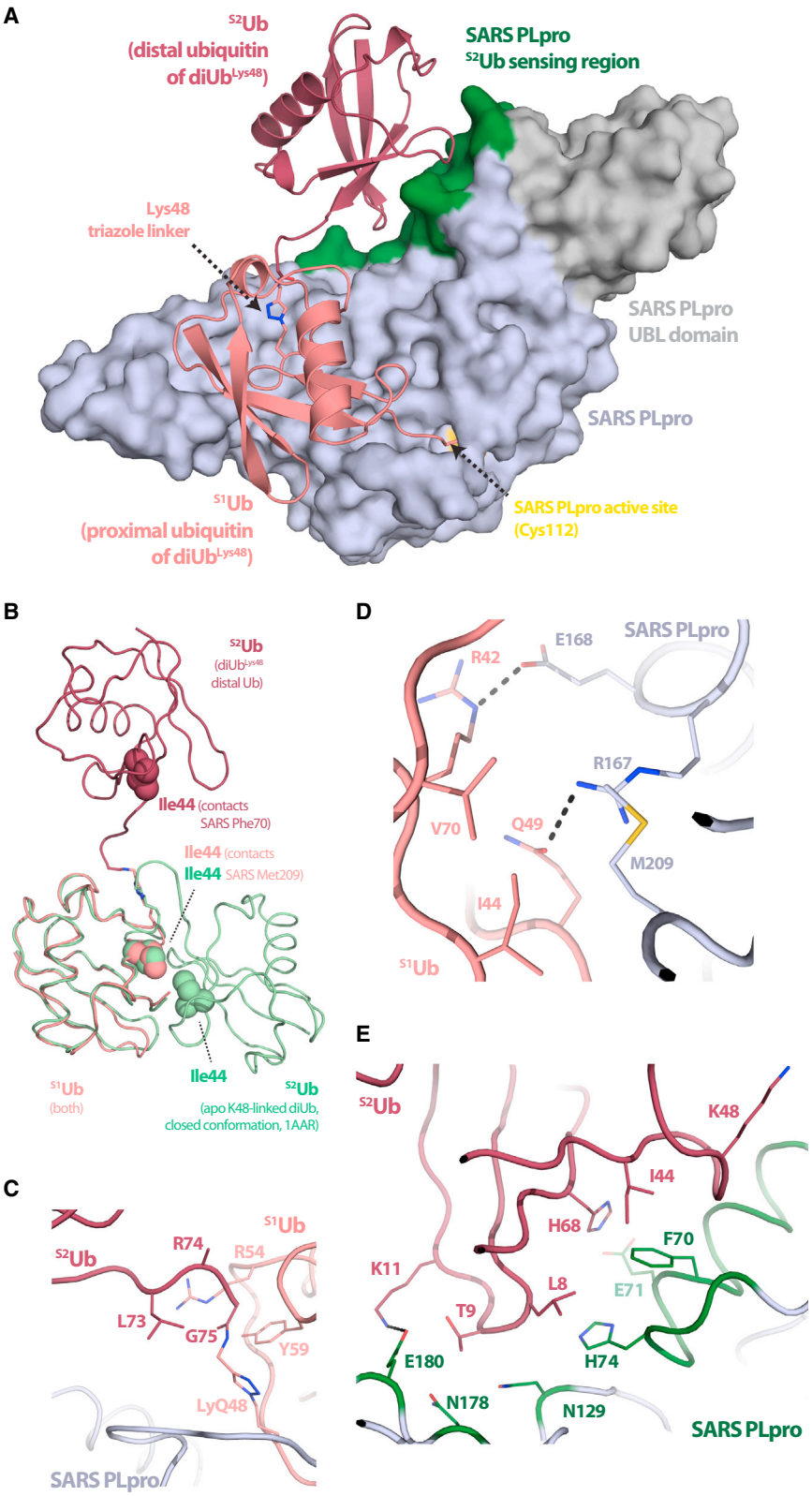


**Figure 2. Crystal Structure of SARS PLpro Bound to a diUb$^{Lys48}$-ABP**

(A) Cartoon and surface representations of SARS PLpro covalently bound to diUb$^{Lys48}$-ABP. SARS PLpro shown in surface representation with the USP-family DUB domain colored blue-white, the N-terminal Ubl domain in gray, the $^{S2}$Ub binding motif in green, and the active site cysteine (C112) in yellow. Cartoon representation of Lys48-linked diUb with proximal Ub ($^{S1}$Ub) in salmon and distal Ub ($^{S2}$Ub) in raspberry.

(B–E) Cartoon representation of interaction surfaces between SARS PLpro and diUb$^{Lys48}$; color as in (A). (B) Structure-based alignment of SARS-PLpro-diUb$^{Lys48}$ and a closed conformation of diUb$^{Lys48}$ (PDB 1AAR). Ub Ile44 (hydrophobic patch) that contact SARS PLpro shown as spheres. (C) View of the covalent triazole linkage between $^{S1}$Ub-Lys48 and $^{S2}$Ub-Gly75 indicating minimal contacts to SARS PLpro. (D) View of contacts between the SARS PLpro palm domain (M209 and Arg167/Asp168) and the $^{S1}$Ub, highlighting both hydrophobic and polar interactions ($^{S1}$Ub-Ile44 and -Gln49/Arg42), respectively. (E) View of contacts between the SARS PLpro $^{S2}$Ub binding motif (Phe70, Glu71, and His74) and the $^{S2}$Ub-Ile44 hydrophobic patch ($^{S2}$Ub-Ile44, -Leu8, and -His68). See also Figure S3.

**Table 1. Crystallographic Data and Refinement Statistics**

| | |
|---|---|
| Data Collection[a] | |
| Source | APS 24IDE |
| Wavelength (Å) | 0.9791 |
| Number of crystals | 1 |
| Space group | $P2_1$ |
| Cell dimensions | |
| a,b,c (Å) | 72.98, 68.24, 119.02 |
| α,β,γ (°) | 90.0, 103.21, 90 |
| Resolution (Å) | 50–2.85 (2.95–2.85) |
| Completeness (%) | 98.0 (100.0) |
| Total reflections | 86,261 (7,690) |
| Unique reflections[a] | 50,843 (5,048) |
| Wilson B-factor | 66.9 |
| Redundancy | 3.3 (3.0) |
| $R_{merge}$ (%) | 7.0 (53.5) |
| $CC_{1/2}$ (%) | 99.7 (57.0) |
| CC[a] (%) | 99.9 (85.2) |
| $< I >/\sigma(I)$ | 13.99 (1.97) |
| Refinement[b] | |
| Resolution (Å) | 50–2.85 (2.95–2.85) |
| Reflections[c] (work/free) | 50,864/2,590 |
| $R_{work}/R_{free}$ (%) | 23.2 (36.5)/26.4 (40.3) |
| Number of atoms | 7366 |
| Protein | 7298 |
| Ligand | 13 |
| Water | 55 |
| Average B factors (Å$^2$) | 79.8 |
| Protein | 79.9 |
| Ligand | 73.6 |
| Water | 58.1 |
| Rmsd | |
| Bond lengths (Å) | 0.003 |
| Bond angles (°) | 0.60 |
| MolProbity[d] | |
| Favored (%) | 93.3 (856) |
| Allowed (%) | 99.7 (853) |
| Outliers (%) | 0.3 (3) |
| Clash score | 100th percentile |
| MolProbity score | 100th percentile |
| PDB code | 5E6J |

[a]Unique reflections for data collected and refinement include anomalous data.
[b]Statistics calculated with Phenix; highest shell in parentheses.
[c]Reflections includes Bijvoet pairs.
[d]Calculated with the program MolProbity.

in Lys48-linked diUb (Figure S3F), despite dissimilar $^{S2}$Ub conformations (Figures 2B and S3G).

Recognition of $^{S2}$Ub involves contacts centered on a hydrophobic interface between the $^{S2}$Ub-Ile44 patch and a SARS PLpro α helix between the palm domain and N-terminal Ub-like (Ubl) domain that spans amino acids 62–74 (Figure 2E). The buried surface area in the $^{S2}$Ub-SARS interface is smaller than the $^{S1}$Ub-SARS interface (~540 Å$^2$ and ~890 Å$^2$, respectively) but includes contacts to $^{S2}$Ub-Ile44, -His68, and -Leu8 by SARS PLpro residues Phe70, Glu71, and His74. $^{S2}$Ub-Lys48 is exposed on the surface (Figure 2E), suggesting that additional Lys48-linked Ub molecules could be accommodated in the context of a polyUb chain. Other contacts to the $^{S2}$Ub core include SARS PLpro residues Asn129, Asn178, and Glu180 from the palm domain, with the latter contacting $^{S2}$Ub-Lys11 (Figure 2E).

## Differential Contributions of $^{S2}$Ub and $^{S1}$Ub Binding Sites for PolyUb$^{Lys48}$ Cleavage

We next queried if proximal and distal Ub recognition are important for Ub chain processing by generating SARS PLpro mutants (Figure S4A) and assaying their activity on polyUb chains. Non-conservative substitutions of a cluster of residues in SARS PLpro that are in proximity to the $^{S2}$Ub-Ile44 hydrophobic patch (e.g., SARS PLpro F70S/E71K/H74G) or individual substitutions F70S and H74G greatly reduce Ub chain cleaving activity by SARS PLpro, as assayed on pentaUb$^{Lys48}$ (Figure 3A, top, green; Figure S4B) and tetraUb$^{Lys48}$ (Figure S4C). In contrast, SARS PLpro N178A/E180K and E180K substitutions, residues that contact $^{S2}$Ub-Lys11, have a less pronounced effect on pentaUb$^{Lys48}$ (Figure 3A, top, green; Figure S4B) or tetraUb$^{Lys48}$ (Figure S4C). These data suggest the importance of distal $^{S2}$Ub contacts, as the $^{S1}$Ub binding surface remains intact in these mutants. Further supporting a dominant role for $^{S2}$Ub interactions is the observation that mutation of residues surrounding the $^{S1}$Ub-Ile44 patch have a modest effect compared to $^{S2}$Ub-Ile44-disrupting mutations for pentaUb$^{Lys48}$ (Figure 3A, bottom, blue; Figure S4B) and tetraUb$^{Lys48}$ (Figure S4C) especially the M209S, R167S, R167S/E168R mutants. The E168R mutant, and a helix-swap mutant that replaces SARS residues with those in MERS PLpro (R167S/E168R+helix), have somewhat diminished activities. And while the N178A/E180K ($^{S2}$Ub-contacting via Lys11) and R167S/E168R+helix mutants ($^{S1}$Ub-contacting via Gln49/Arg42) display diminished polyUb cleaving ability, their defects are less than that observed for the F70S/E71K/H74G ($^{S2}$Ub-contacting via Ile44) mutant. The catalytic mutant (C112A) has no activity.

The relative contribution of $^{S1}$Ub and $^{S2}$Ub interactions within SARS PLpro was further probed by monitoring cleavage activity using tetraUb$^{Lys48}$ where cleavage depends on binding via S2-S1 (Figure 3B, top) and comparing this to diUb$^{Lys48}$ cleavage reactions that depend on binding via S1-S1′ (Figure 3B, bottom). It is worth noting that diUb$^{Lys48}$ cleavage by SARS PLpro requires 5-fold higher concentration of enzyme compared to tetraUb$^{Lys48}$ to observe activity. SARS PLpro wild-type (WT) activities were also compared to enzymes carrying mutations in the $^{S1}$Ub and $^{S2}$Ub binding sites using Lys48-linked diUb$^{Lys48}$ and tetraUb$^{Lys48}$ substrates (Figures 3C and 3D). As expected, the SARS PLpro $^{S2}$Ub mutant (F70S/E71K/H74G) exhibits diminished activity against tetraUb$^{Lys48}$ (Figure 3C, top) yet retains WT-level activity on diUb$^{Lys48}$ (Figure 3C, bottom). Thus, $^{S2}$Ub recognition is dispensable for diUb$^{Lys48}$ cleavage, consistent with an S1-S1′ binding mode being relevant for diUb$^{Lys48}$ cleavage. In contrast,

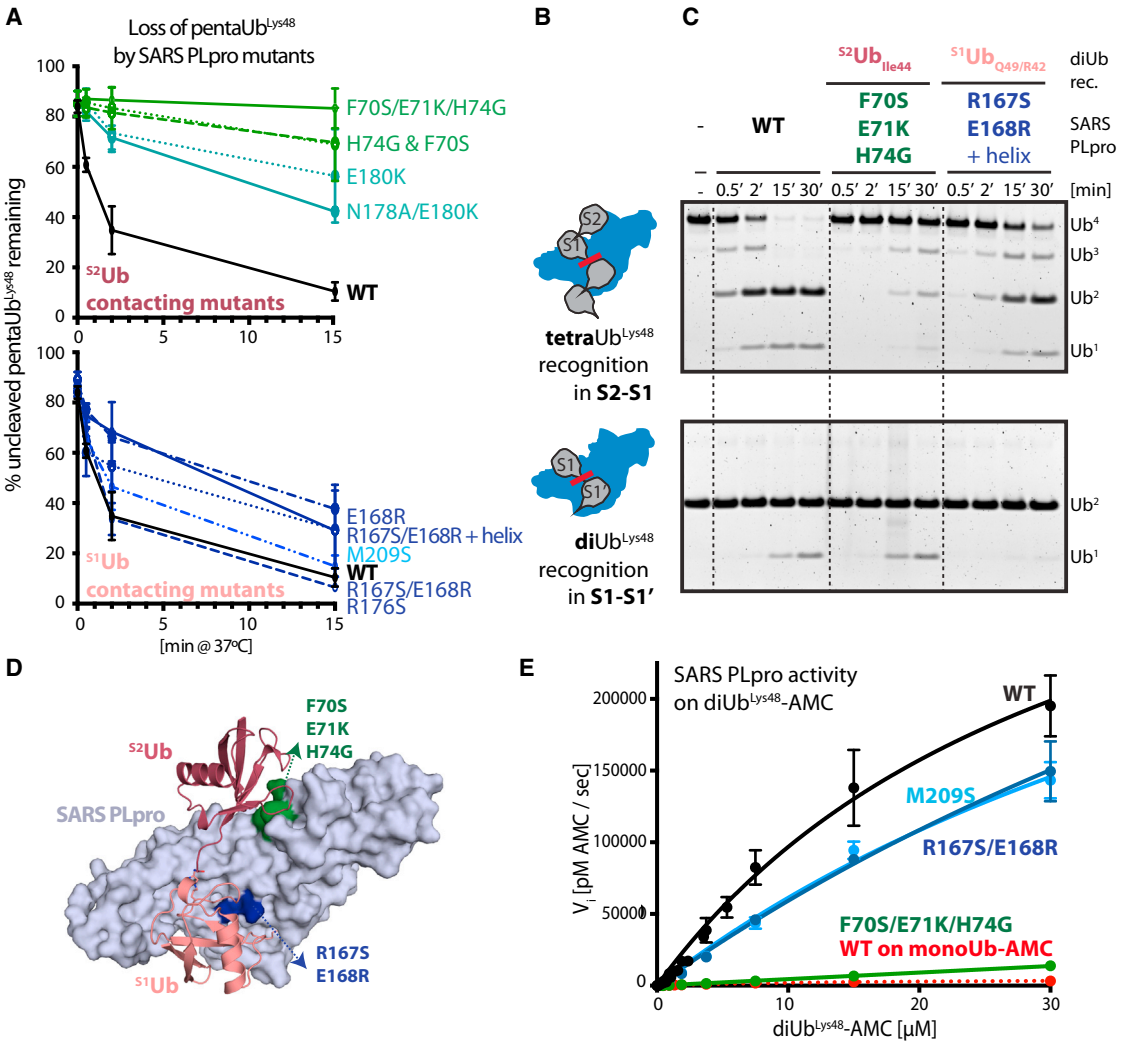


**Figure 3. Contribution of SARS PLpro $^{S1}$Ub and $^{S2}$Ub Sites to polyUb$^{Lys48}$ Cleavage**

(A) Ub chain cleavage activities of SARS PLpro WT (black) and its mutants ($^{S2}$Ub, top, green; $^{S1}$Ub, bottom, blue) on pentaUb$^{Lys48}$. Representative gels used to derive graphs shown in Figure S3B. Error bars represent ±SEM.

(B) Schematics of tetraUb$^{Lys48}$ and diUb$^{Lys48}$ recognition by SARS PLpro.

(C) Gel-based cleavage assays of SARS PLpro WT and mutants on tetraUb$^{Lys48}$ (top) and diUb$^{Lys48}$ (bottom) indicating differential effects of diUb $^{Lys48}$ and tetraUb $^{Lys48}$ cleaving activities for $^{S1}$Ub and $^{S2}$Ub mutants of SARS PLpro. Additional mutants analyzed in Figure S4C.

(D) Cartoon and surface representation of SARS-PLpro~diUb$^{Lys48}$ indicating the location of the $^{S1}$Ub and $^{S2}$Ub mutants.

(E) Michaelis-Menten kinetics of WT (black) and selected SARS PLpro mutants (M209S, hydrophobic S1 mutant, light blue; R167S/E168R, polar S1 mutant, dark blue; F70S/E71K/H74G, S2 mutant, green) on diUb$^{Lys48}$-AMC substrates and comparison to SARS PLpro WT on monoUb-AMC (in red). Extracted kinetic parameters ($k_{cat}$ and $K_M$) are in Table 2.

See also Figure S4.

the $^{S1}$Ub mutant (R167S/E168R+helix) has diminished diUb$^{Lys48}$ cleavage activity yet retains the ability to cleave tetraUb$^{Lys48}$ chains with characteristic accumulation of diUb intermediates (Figure 3C). Single point mutants of the composite mutants (F70S for $^{S2}$Ub, E168R for $^{S1}$Ub) exhibit similar cleavage profiles (Figure S4C). These results suggest that mutations predicted to disrupt $^{S1}$Ub recognition do not prevent cleavage of tetraUb$^{Lys48}$ when an intact $^{S2}$Ub binding surface is present. As earlier, mutations within SARS PLpro predicted to disrupt contacts to $^{S2}$Ub near Lys11 have a modest effect on tetraUb$^{Lys48}$ cleavage, and combining mutations designed to disrupt both $^{S2}$Ub-Ile44 and -Lys11 patches are not additive (data not shown). Additionally, mutations designed to disrupt contacts to $^{S2}$Ub, alone or in combination, do not display gain-of-function activity toward diUb$^{Lys48}$, suggesting that disrupting $^{S2}$Ub interaction does not convert SARS PLpro into a DUB with stronger preference for S1-S1′ binding.

To quantify the contribution of $^{S2}$Ub and $^{S1}$Ub contacts with respect to diUb$^{Lys48}$ recognition by SARS PLpro, we turned to recently developed fluorogenic model diUb$^{Lys48}$-AMC

**Table 2. Kinetic and Inhibition Parameters for SARS PLpro and Its Mutants on -AMC Substrates**

| SARS PLpro Mutant | Kinetic Parameter | MonoUb-AMC | Triazole Linked $DiUb^{Lys48}$-AMC | Native $DiUb^{Lys48}$-AMC | ISG15-AMC |
|---|---|---|---|---|---|
| WT | Apparent $k_{cat}/K_M$ [$M^{-1}s^{-1}$] | 3.33E+04 | 1.26E+06 | 1.01E+06[a] | 5.98E+05 |
| | $k_{cat}$ [$s^{-1}$] | 0.5042 ± 0.02839 | 42.02 ± 3.872 | n/a | 9.533 ± 1.218 |
| | $K_M$ [μM] | 15.12 ± 1.747 | 33.42 ± 4.869 | n/a | 15.94 ± 3.172 |
| | Fold $k_{cat}/K_M$ over monoUb-AMC | 1.00 | 37.70 | 30.33[a] | 17.93 |
| | Michaelis-Menten curve fit ($R^2$) | 0.9845 | 0.9668 | n/a | 0.9411 |
| F70S E71K H74G (S2 mutant) | $k_{cat}/K_M$ [$M^{-1}s^{-1}$] | — | 4.23E+04[a] | — | 2.94E+05 |
| | $k_{cat}$ [$s^{-1}$] | — | n/a | — | 2.748 ± 0.6693 |
| | $K_M$ [μM] | — | n/a | — | 9.359 ± 3.547 |
| | % $k_{cat}/K_M$ of WT (per substrate) | — | 3.37 | — | 49.10 |
| R167S E168R (S1 polar mutant) | $k_{cat}/K_M$ [$M^{-1}s^{-1}$] | — | 6.50E+05 | — | 3.64E+04 |
| | $k_{cat}$ [$s^{-1}$] | — | 65.56 ± 22.38 | — | 0.318 ± 0.1184 |
| | $K_M$ [μM] | — | 100.8 ± 42.49 | — | 8.764 ± 5.614 |
| | % $k_{cat}/K_M$ of WT (per substrate) | — | 51.63 | — | 6.08 |
| M209S (S1 hydrophobic mutant) | $k_{cat}/K_M$ [$M^{-1}s^{-1}$] | — | 7.06E+05 | — | 4.20E+05 |
| | $k_{cat}$ [$s^{-1}$] | — | 46.59 ± 10.29 | — | 4.774 ± 1.263 |
| | $K_M$ [μM] | — | 66.01 ± 19.61 | — | 11.88 ± 4.578 |
| | % $k_{cat}/K_M$ of WT (per substrate) | — | 56.13 | — | 67.19 |
| WT | $K_i$ [μM] with monoUb[b] | NI | NI | NI | NI |
| | $K_i$ [μM] with $diUb^{Lys48}$ | 2.26 (0.9265) | 9.05 (0.8942) | 12.07 (0.8892) | 3.31 (0.8351) |
| | $K_i$ [μM] with $triUb^{Lys48}$ | — | 10.57 (0.9509) | 10.11 (0.9066) | 4.08 (0.6709) |
| | $K_i$ [μM] with ISG15 | NI | NI | NI | NI |

n/a, not applicable ($k_{cat}$ and $K_M$ cannot be independently calculated); NI, no detectable inhibition ($IC_{50}$ > 100 μM or data do not converge).
[a]Substrate not saturated, $k_{cat}/K_M$ calculated from slope of linear graph.
[b]$K_i$ values were derived from $IC_{50}$ values based on the equation $K_i = IC_{50}/(S/K_M+1)$, assuming competitive inhibition, where S is the concentration of the substrate (based on Cer et al., 2009). Brackets show goodness of fit ($R^2$) of $IC_{50}$ values obtained from Prism's log(inhibitor) versus normalized curve fit. Inhibition curves are shown in Figure S6A.

substrates (containing a triazole-linker between Ub moieties), where the AMC fluorophore is conjugated to the proximal end of $diUb^{Lys48}$ (Flierman et al., 2016), enabling kinetic characterization of SARS PLpro by monitoring fluorescence during hydrolysis of the -AMC amide bond. Michaelis-Menten kinetic analysis of monoUb- and $diUb^{Lys48}$-AMC cleavage by SARS PLpro and its selected $^{S2}$Ub and $^{S1}$Ub mutants reveals that SARS PLpro cleaves the $diUb^{Lys48}$-AMC about ~37-fold more efficiently than it cleaves monoUb-AMC (Figure 3E, black and red, respectively; Table 2, compare apparent $k_{cat}/K_M$ values of 3.3E+04 $M^{-1}s^{-1}$ for monoUb-AMC to 1.26E+06 $M^{-1}s^{-1}$ for $diUb^{Lys48}$-AMC). Moreover, kinetic comparison of SARS PLpro mutants reveals that loss of S2 interactions (F70S/E71K/H74G; Figure 3E, green; Table 2) results in an ~33-fold loss of catalytic efficiency ($k_{cat}$ and $K_M$ could not be measured independently, and the S2 mutant could not be saturated by the $diUb^{Lys48}$-AMC substrate, indicative of a binding defect). Thus, the S2 mutant converts SARS PLpro into an S1-dependent, monoUb-based DUB. In contrast, mutation of either the hydrophobic interaction in the $^{S1}$Ub site (M209S, Figure 3E, light blue; Table 2) or polar contacts to $^{S1}$Ub (R167S/E168R, Figure 3E, dark blue; Table 2) results in a modest decrease in catalytic efficiency, an effect mainly driven by a 2- to 3-fold increase in $K_M$ without a corresponding loss in $k_{cat}$ (Table 2). Assaying additional point mutants at a single monoUb- or $diUb^{Lys48}$-AMC substrate concentration mirrors these trends (Figure S4D, top). Importantly, S2 mutants do not exhibit diminished monoUb-AMC cleavage rates (Figure S4D, bottom), consistent with gel-based experiments, as they maintained activity when processing $diUb^{Lys48}$ into monoUb.

Structure-based alignment of the Lys48 linkage visible in the triazole-linked $diUb^{Lys48}$-ABP~SARS-PLpro crystal structure to native Lys48 in free $diUb^{Lys48}$ (PDB: 1AAR) suggests that the triazole-linkage mimics the distance and geometry of a native isopeptide-bond (Figure S4E). To test if the triazole linkage is a good functional mimic of the native isopeptide-bond, we generated a native isopeptide-linked $diUb^{Lys48}$-AMC reagent (Figure S4F) and assayed initial cleavage rates for triazole-linked and native $diUb^{Lys48}$-AMC substrates (Figure S4G). Results indicate that the triazole linker is a faithful mimic of the isopeptide bond as initial cleavage rates are similar (despite native $diUb^{Lys48}$-AMC being contaminated with monoUb-AMC precursor; see Figure S4F).

SARS PLpro could not be saturated using the native substrate due to insufficient quantities, so inhibition studies were performed with triazole-linked or native isopeptide $diUb^{Lys48}$-AMC as substrates to calculate inhibition constants ($K_i$) using Lys48-linked Ub chains as inhibitors. Results in Table 2 (see also Figure S6A for inhibition curves) show that $diUb^{Lys48}$ and $triUb^{Lys48}$

inhibit triazole-linked or native diUb$^{Lys48}$-AMC cleavage with comparable $K_i$ values (9 and 10 μM or 12 and 10 μM, respectively), values just ~3-fold lower than the $K_M$ for diUb$^{Lys48}$-AMC as determined by Michaelis-Menten kinetics. Additionally, diUb$^{Lys48}$ inhibited monoUb-AMC hydrolysis with a $K_i$ of ~2.2 μM, a result consistent with kinetic assays where diUb$^{Lys48}$ recognition is preferred over monoUb. We were unable to observe inhibition of cleavage of diUb$^{Lys48}$-AMC substrates using monoUb or free ISG15 (Table 2).

Collectively, these results support the conclusion that distal $^{S2}$Ub and proximal $^{S1}$Ub binding surfaces are important for SARS PLpro activity, with $^{S2}$Ub interactions being dominant, and that polyUb contacts to S2-S1 surfaces are preferred over interactions with S1-S1′ when processing Lys48-linked Ub chains.

## S2-S1 Recognition by SARS PLpro Underlies Lys48 Ub Chain Linkage Specificity

DiUB can be linked via seven Ub lysine residues as well as its N terminus to alter their topology. Although dynamic, diUb conformations can be stabilized by interactions between Ub molecules, sometimes templated by their interacting partners (Ye et al., 2012). Linkage specificity for most DUBs characterized thus far is determined by contacts across the protease active site with diUb occupying S1-S1' sites (Keusekotten et al., 2013; Mevissen et al., 2013; Sato et al., 2008, 2015). As shown previously, SARS PLpro is poor at cleaving diUb and does not strictly require a specific linkage across S1-S1′ (Békés et al., 2015). Given the extended conformation of diUb$^{Lys48}$ observed in complex with SARS PLpro and the paucity of contacts to the diUb$^{Lys48}$ linkage (Figure 2C), we hypothesized that SARS PLpro might indirectly sense linkage specificity by requiring that diUb occupies both $^{S2}$Ub and $^{S1}$Ub sites, a requirement that would place limits on the type of chain that could be accommodated because of differences in chain topology and distance between individual Ub molecules relative to the two Ub binding sites.

To assess S2-S1 linkage specificity of SARS PLpro, we tested a panel of linkage-specific distal diUb-ABPs to covalently label SARS PLpro. Although not as efficient as diUb$^{Lys48}$-ABP, diUb$^{Lys27}$-ABP exhibited better labeling efficiency compared other linkage-specific diUb-ABPs, which reacted at levels similar to monoUb-ABP (Figure 4A and S5A). Since covalent activity-based probes are very reactive, we also tested linkage-specific diUb-AMC substrates by analyzing initial cleavage rates by SARS PLpro. These results suggest that SARS PLpro activity is highly restricted to diUb$^{Lys48}$-AMC cleavage (Figures 4B and S5B) as diUb$^{Lys48}$-AMC is cleaved ~100-fold faster compared to other linkages. Each chain-forming residue in $^{S1}$Ub is available for conjugation in our diUb$^{Lys48}$-SARS PLpro complex (Figure 4C), but the distance between $^{S1}$Ub-Lys48 and the SARS-Phe70 $^{S2}$Ub binding site is closest (26 Å) with each of the other sites requiring an additional 10 to 15 Å to span between the conjugated lysine and $^{S2}$Ub binding site (Figure S5C). This raised the possibility that linkage-specificity across S2-S1 is enforced by restricting access to other topologies by requiring that SARS PLpro read the distance between diUb Ile44 hydrophobic patches via S2-S1 (Figure 2B), a requirement that is only satisfied by chains carrying Lys48 linkages. Accordingly, assaying homotypic linkage-specific tetra-ubiquitin (tetraUb) chains in endpoint cleavage assays also confirmed SARS PLpro to be Lys48-specific (Figure 4D).

## SARS PLpro Lys48 Specificity Is Also Aided by S1-S1′ Interactions

Most linkage-specific DUBs characterized to date rely on S1-S1′ interactions to achieve linkage-specificity, although OTUD2 and OTUD3 have been shown to utilize both S2-S1 and S1-S1′ interactions to mediate Lys11- and Lys6/11-specificity, respectively (Mevissen et al., 2013). We noticed greater defects for diUb$^{Lys48}$-AMC cleavage for some SARS PLpro mutants (especially E180K, N178A/E180K, E168R, and R67S/E168R+helix) compared to gel-based assays using polyUb$^{Lys48}$ substrates. As diUb$^{Lys48}$-AMC requires only S2-S1 interactions for cleavage, we wondered if additional interactions outside S2-S1 might be responsible for the residual specificity and activity observed for cleavage of polyUb$^{Lys48}$ substrates.

To determine if a Lys48-linkage was also preferred across S1-S1′ (Figure 4E), we assayed SARS PLpro and its $^{S2}$Ub-Ile44 mutant (F70S/E71K/H74G) for cleavage of homotypic Lys48- and Lys63-linked tetraUb chains and a mixed linkage tetraUb chain consisting of two Lys48-linked dimers linked by Lys63 (see schematics in Figure 4F). This latter mixed chain could be recognized by SARS PLpro in S2-S1, but its cleavage would require accommodation of a Lys63-linkage across S1-S1′. A time course reveals that SARS PLpro readily cleaves homotypic Lys48 tetraUb chains but is inactive on homotypic Lys63 tetraUb chains. Interestingly, the mixed chain is cleaved when the Lys63 linkage is presented across S1-S1′, but only when an intact S2 site is present (Figure 4G). Initial cleavage rates (Figure 4H) show that SARS PLpro is ~5-fold slower in cleaving the mixed chain compared to the homotypic Lys48-linked chain, suggesting some specificity for a Lys48 linkage across S1-S1′. More importantly, the $^{S2}$Ub-Ile44 mutant exhibits faster cleavage rates on homotypic Lys48 chains than on mixed or on homotypic Lys63-linked chains (Figures 4G and 4H). Taken together, these data suggest a measurable specificity for Lys48 across S1-S1′, even when diUb$^{Lys48}$ recognition via S2-S1 is compromised. Thus, Lys48-specificity of SARS PLpro is enforced by S2-S1 recognition but complemented by a preference for Lys48 linkages across S1-S1′, suggesting that SARS PLpro would be most active on polyUb$^{Lys48}$ chains. Consistent with the hypothesis of S2-S1-S1′ recognition of polyUb$^{Lys48}$ chains, di- and monoUb-conjugated IκBα accumulates during cleavage by SARS PLpro (Figure 1D, IκBα), while unmodified IκBα remains static (Figure 1D, lighter exposure IκBα). These data suggest that SARS PLpro acts efficiently on polyUb$^{Lys48}$ chains in a diUb-dependent manner yet generates mono- and diUb-conjugated substrate remnants that may no longer represent its preferred substrate.

In the absence of a crystal structure of a diUb$^{Lys48}$ unit occupying S1-S1′ sites of SARS PLpro, we analyzed our structure for loops predicted to be proximal to S1′ within SARS PLpro that differ in sequence from MERS PLpro, which displays little linkage-specificity across S1-S1′ (Békés et al., 2015). We identified two residues, W107 and A108, adjacent to the exit tunnel of the SARS PLpro active site and mutated them to residues

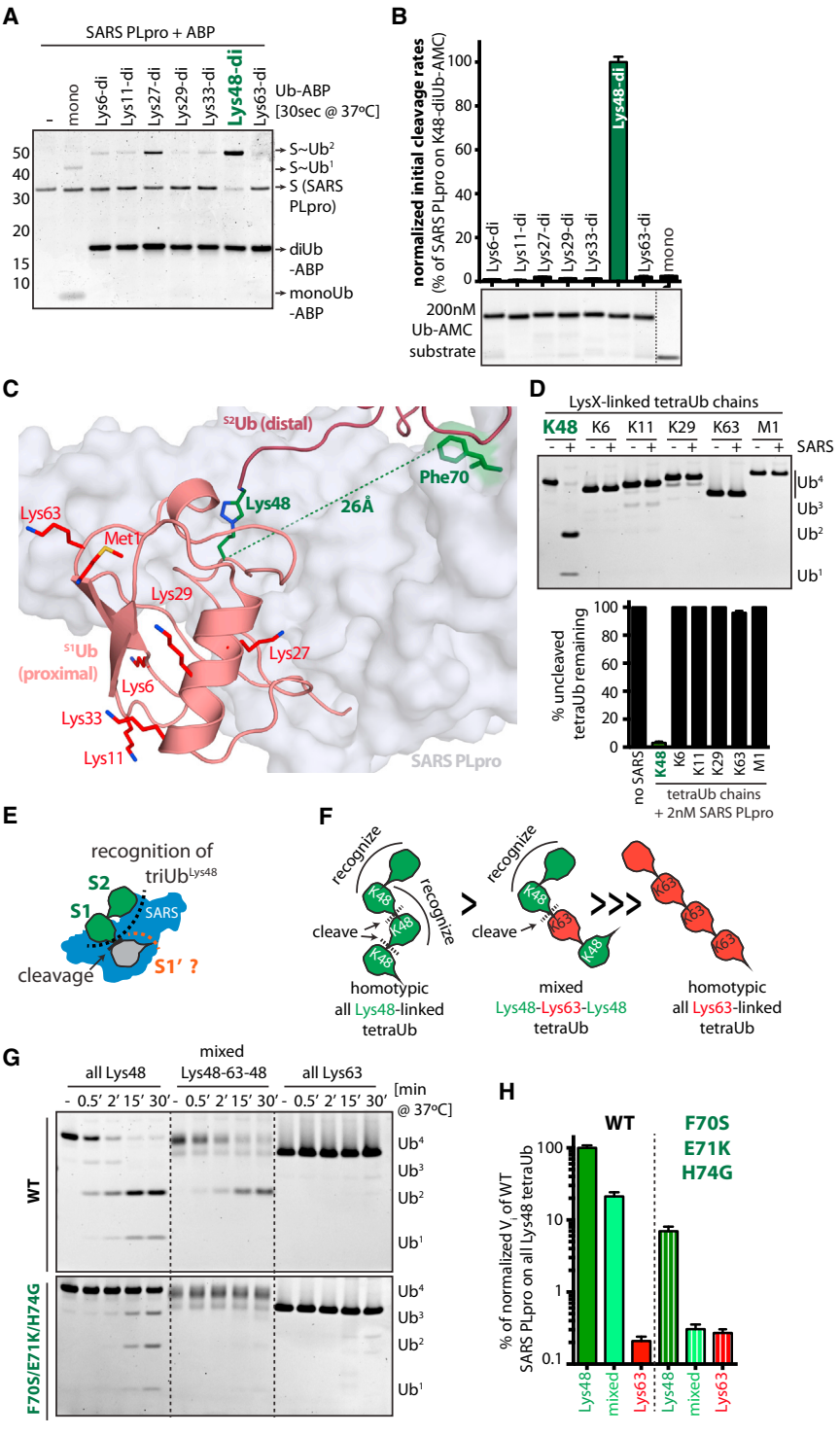


**Figure 4. SARS PLpro Activity Is Restricted to Lys48-Linked Ub Chains with Specificity Dominated by S2-S1 Interactions**

(A and B) S2-S1 linkage specificity of SARS PLpro probed by (A) SDS-PAGE analysis of cross-linking to linkage-specific diUb-ABPs (SYPRO-stained) and (B) release of AMC using diUb-AMC fluorogenic substrates with initial linear cleavage rates ($V_i$) plotted as percent of diUb$^{Lys48}$-AMC cleavage rate by WT SARS PLpro as derived from curves in Figure S4B.

(C) View of SARS-PLpro∼diUb$^{Lys48}$-ABP highlighting the location of $^{S1}$Ub-Lys48 (dark green, sticks) and its proximity to Phe70 (green) in the SARS PLpro $^{S2}$Ub binding site. Other chain-forming $^{S1}$Ub residues (Lys-6, -11, -27, -29, -33, and -63 and Met1) shown as sticks (red).

(D) Linkage specificity of SARS PLpro assayed using homotypic tetraUb chains. Representative gel shown and bar graph indicating ±SEM from duplicate experiments.

(E) Schematics of triUb$^{Lys48}$ chain recognition by SARS PLpro via S2-S1 (green) and S1′ (gray).

(F) Cartoon of tetraUb chains, indicating SARS PLpro preferred sites of recognition (curved line) and cleavage (dotted line).

(G) Time-course for cleavage of tetraUb chains by SARS PLpro and its S2 mutant.

(H) Quantification of $V_i$ as determined from duplicate experiments in Figure 4G. Error bars represent ±SEM.

See also Figure S5.

observed in MERS PLpro (Figure S5D). Cleavage assays with this putative S1′ mutant reveals that W107L/A108S has diminished activity on triUb$^{Lys48}$, which requires interactions with S2-S1-S1′ (Figures S5E and S5F), but exhibits no significant loss of activity when cleaving diUb$^{Lys48}$-AMC, a substrate that is solely dependent on S2-S1 (Figure S5F). This mutant, however, loses activity on Ub-AMC and ISG15-AMC (whose recognition is primarily S1 dependent). Combined with the observation that a Lys48-linked isopeptide is preferred as a substrate, these data suggest that S1′-dependent recognition of Lys48-linkages by SARS PLpro is possible, although additional work will be required to explore this hypothesis.

## Recognition of DiUb$^{Lys48}$ and ISG15 Requires Distinct Elements within SARS PLpro

ISG15 is a tandem ubiquitin-like (Ubl) molecule consisting of two Ubl folds linked by a flexible hinge (Narasimhan et al., 2005). ISG15 is implicated in antiviral immunity, and it is a preferred substrate of SARS PLpro when compared to monoUb. Indeed, ISG15-AMC is cleaved ∼20-fold faster than Ub-AMC (Table 2) (Békés et al., 2015; Lindner et al., 2007; Ratia et al., 2014). DiUb$^{Lys48}$-AMC (apparent $k_{cat}/K_M$ of 1.26E+06 $M^{-1}s^{-1}$) is only preferred by ∼2-fold compared to ISG15-AMC (apparent $k_{cat}/K_M$ of 5.98E+05 $M^{-1}s^{-1}$), suggesting that the preferred substrate for SARS PLpro is Lys48-linked polyUb chains.

The activity of SARS PLpro on ISG15 has been shown to be dependent on the distal Ubl within ISG15 (Lindner et al., 2007). Because the S2 binding site is important for diUb$^{Lys48}$ cleavage as described here and as proposed previously (Ratia et al., 2014), we sought to directly compare mutations in S2 and S1 of SARS PLpro and their impact on ISG15 cleavage activity. SARS PLpro $^{S1}$Ub and $^{S2}$Ub mutants were used to cleave ISG15-AMC using Michaelis-Menten kinetics (Figure 5A). Mutations have contrasting effects for ISG15-AMC cleavage (Figure 5A; Table 2). The S1 polar mutant (Figure 5A, dark blue) exhibits greater defects for ISG15-AMC cleavage with minimal effects diUb$^{Lys48}$-AMC cleavage. In contrast, the S2 mutant exhibits major defects for diUb$^{Lys48}$-AMC cleavage with less severe defects in ISG15-AMC cleavage. To confirm these differential effects, we utilized lysates prepared from IFNβ/MG132-treated cells that contained polyUb$^{Lys48}$ chains and ISG15-conjugated substrates and added recombinant SARS PLpro mutants (Figure 5B). Analyzing loss of HMW polyUb$^{Lys48}$-conjugates and the appearance of free ISG15, indicative of cleavage of ISGylated substrates, reveals contrasting effects for S2 and S1 mutants (Figure 5C). While the S2 mutant compromises polyUb$^{Lys48}$ chain, but not ISG15 cleavage, the S1 mutant has the opposite effect. Finally, we compared other SARS PLpro mutants for cleavage of diUb$^{Lys48}$-AMC and ISG15-AMC (Figure S6B). Overall, $^{S2}$Ub site mutants (green) show minimal loss of ISG15-AMC cleavage activity, while $^{S1}$Ub mutants (blue), particularly those containing the E168R mutation, have a pronounced loss-of-function effect. Thus, ISG15 recognition appears more dependent on interactions within S1 and perhaps an alternative S2, while diUb$^{Lys48}$ recognition is more dependent on contacts within S2. It is difficult to rationalize these effects in the absence of a structure of ISG15 bound to SARS PLpro, but it appears clear that ISG15 recognition differs in details when compared to diUb$^{Lys48}$ recognition (Figure S6C).

## DISCUSSION

SARS PLpro appears unique among viral and human DUBs characterized thus far in its ability to recognize polyUb chains by reading units of a Lys48-linked diUb (Békés et al., 2015). Here, we reveal the structural basis for diUb$^{Lys48}$ recognition and specificity by SARS PLpro. Coupled with mutational, biochemical and kinetic data, our structure helps to explain the strict Lys48-linkage specificity exhibited by this viral DUB, which is primarily enforced by engaging the diUb module within S2-S1, and enhanced by a slight preference for Lys48-linked Ub across S1-S1′ (Figure 5D). To our knowledge, the diUb$^{Lys48}$-SARS PLpro structure represents the only available structure of a linkage-specific DUB bound to a Lys48-linked Ub chain, a result enabled by recently developed diUb activity-based probes (Flierman et al., 2016).

Instead of relying on diUb recognition across S1-S1′, as is common among other DUBs (Keusekotten et al., 2013; Mevissen et al., 2013; Sato et al., 2015) and endoproteases (Berger and Schechter, 1970), SARS PLpro recognizes diUb across S2-S1 binding surfaces that are tuned to recognize Lys48-linked Ub chains. This mode of Ub chain recognition has only been reported for the catalytic core of OTUD2, where an additional binding site mediates interaction with a Lys11-linked diUb (Mevissen et al., 2013). Through modeling, mutational analysis, and the crystal structure of a monoUb-bound SARS PLpro, the Mesecar group suggested that SARS PLpro is an S2-S1 mode DUB (Ratia et al., 2014) and that the distal Ub would be recognized by a hydrophobic surface in SARS PLpro, involving Phe70. Our current study illuminates the structural basis for this interaction. We provide biochemical evidence that the $^{S2}$Ub interface has a dominant role in diUb$^{Lys48}$ recognition and polyUb chain cleaving activity, since mutating the distal $^{S2}$Ub recognition surface is more detrimental than disrupting the proximal $^{S1}$Ub recognition surface. We also provide evidence that SARS PLpro Lys48-specificity is complemented by a preference for Lys48-linked chains across S1-S1′.

The hydrophobic patches in Ub proteins are usually packed against each other in free Ub$^{Lys48}$ chains (Fushman and Wilkinson, 2011). In the diUb$^{Lys48}$-SARS PLpro complex, diUb$^{Lys48}$ exhibits an extended conformation, with Ub hydrophobic patches separated by ~30 Å and recognized by contacts provided by the $^{S1}$Ub and $^{S2}$Ub sites in the diUb$^{Lys48}$-SARS PLpro complex. As Ub chains are dynamic in solution (Ye et al., 2012), and because SARS PLpro is structurally similar in apo, monoUb, and diUb$^{Lys48}$ complexes, it is likely that SARS PLpro captures diUb units in this conformation.

While SARS PLpro exhibits an ~5-fold preference for a Lys48-linkage in the S1-S1′ binding mode when an S2 site is also occupied, a lax requirement at S1′ is consistent with its function as an endopeptidase for viral pre-protein processing and perhaps cleavage of ISG15 substrates. The biological targets of SARS PLpro remain unclear, but the preference for polyUb$^{Lys48}$ chain cleavage into units of diUb$^{Lys48}$ suggests it is likely targeted to substrates that are modified by Lys48-linked polyUb chains.

The diUb-based recognition exhibited by SARS PLpro suggests that SARS PLpro could stabilize monoUb-modified substrate products (Békés et al., 2015), as they are not preferred substrates for SARS PLpro. Indeed, cleavage of Lys48-linked polyUb chains from IκBα by SARS PLpro led to an increase in di- and monoUb-conjugated forms of IκBα. Whether SARS PLpro cleaves other polyUb$^{Lys48}$-conjugated substrates to di- or monoUb-conjugated forms remains to be determined. Mono-ubiquitination at membranes and at the endoplasmic reticulum (ER) has been shown to regulate endocytosis and vesicle trafficking (Clague et al., 2012), which are also involved in coronavirus propagation. Given that SARS PLpro is ER localized, it is possible that SARS PLpro functions to stabilize mono-Ub "stubs" on ER substrates to provide an unknown advantage for the virus.

It remains unclear if the anti-inflammatory properties of SARS PLpro require all or a combination of its endopeptidase, DUB, or deISGylating activities. With mutations described herein, which bias activities in deubiquitination versus deISGylation, it may be possible to discern if both activities are important during SARS infection. With that said, it is worth noting that SARS viral titer levels peak at 16–20 hr in cell culture and in mouse model infection studies (Channappanavar et al., 2016; Totura and Baric, 2012), while interferon (IFN)-responsive genes, such as ISG15, are only induced later during infection (Channappanavar et al.,

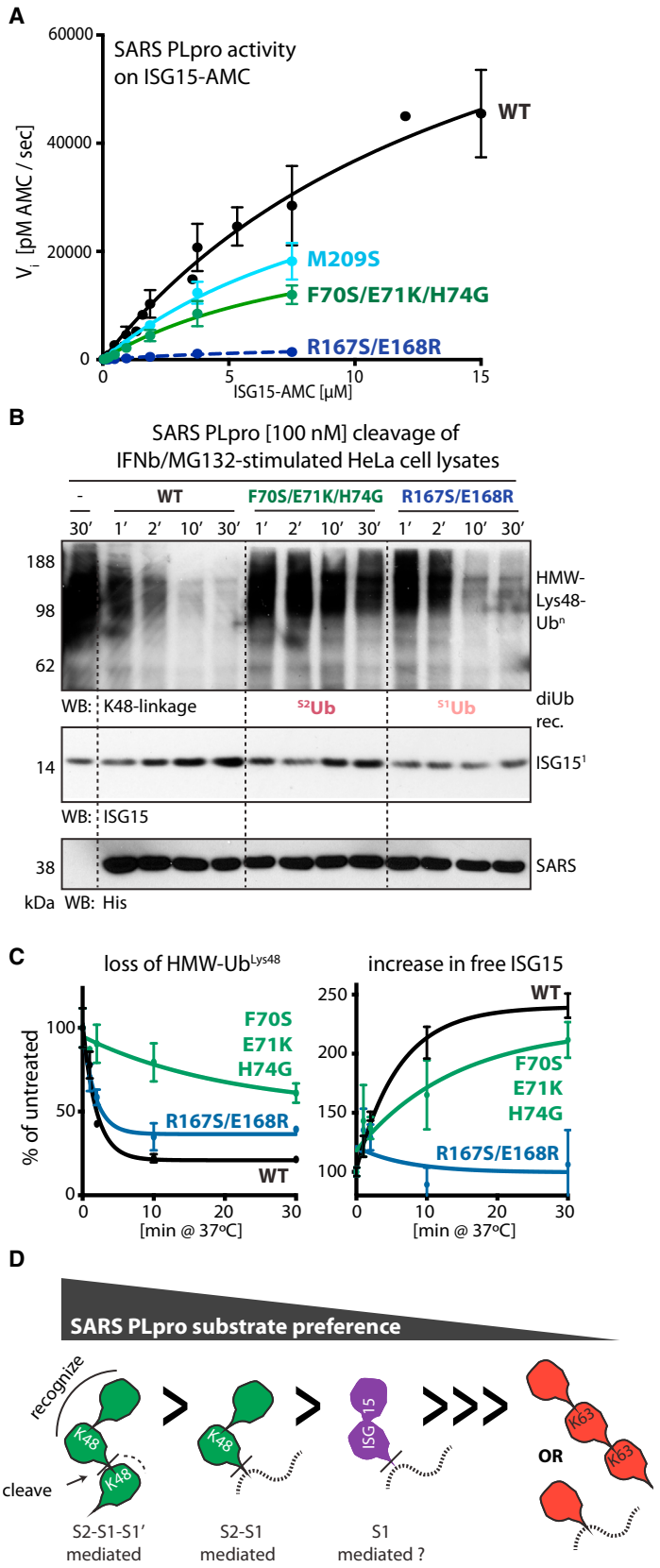


**Figure 5. Recognition of DiUb$^{Lys48}$ and ISG15 by SARS PLpro Appears Distinct**

(A) Michaelis-Menten kinetics of WT (black) and selected SARS PLpro mutants (M209S, S1 mutant, light blue; R167S/E168R, S1 mutant, dark blue; F70S/E71K/H74G, S2 mutant, green) using ISG15-AMC. Extracted kinetic parameters ($k_{cat}$ and $K_M$) in Table 2.

(B) Cleavage of HMW-Ub$^{Lys48}$ (top, WB anti-K48) and ISG15-conjugates (bottom, WB ISG15) in lysates prepared from IFNβ/MG132-treated cells by SARS PLpro WT and S2 and S1 mutants.

(C) Quantification of loss of HMW-Ub$^{Lys48}$ (left) and appearance of free ISG15 (right) from duplicate experiments shown in Figure 5B. Error bars represent ±SEM.

(D) Schematic representation of SARS PLpro substrate specificity. Dashed lines can indicate the -AMC substrate, a non-Lys48-linked Ub unit, or a protein substrate.

See also Figure S6.

2016). As such, it is likely that the virus has already achieved its full replicative potential before SARS PLpro would encounter ISG15. Additionally, the function of substrate-conjugated ISG15 in anti-viral immunity in humans is now in question (Bogunovic et al., 2012), as a non-conjugatable form of ISG15 was shown to have similar activities as WT ISG15, likely via stabilization of USP18 (Zhang et al., 2015). Given the preference for polyUb$^{Lys48}$ and diUb$^{Lys48}$ over ISG15, it appears likely that polyUb$^{Lys48}$-conjugated substrates are the primary cellular targets of SARS PLpro. These observations suggest that SARS PLpro activities against ISG15 targets may not be as relevant for coronavirus infection as previously thought.

Although the identity of true SARS PLpro substrates remains to be determined, they could include host factors involved in anti-viral signaling, such as IκBα, or viral proteins targeted for degradation by host anti-viral E3 ligases. We propose a model where the most favored substrates for SARS PLpro would be Lys48-linked polyUb chains (S2-S1-S1′ dependent), followed by diUb$^{Lys48}$-conjugates (S2-S1 dependent), followed by ISG15-conjugates, with the least favored substrates being monoUb-conjugated substrates and other polyUb chains (only S1 dependent) (Figure 5D).

## EXPERIMENTAL PROCEDURES

### Synthesis of the Singly Biotinylated TriUb$^{Lys48}$ Substrate

Biotinylated triUb$^{Lys48}$ was generated using procedures based on previously reported protocols (El Oualid et al., 2010) with modification described in Supplemental Experimental Procedures.

### Cloning, Protein Expression, Purification, Crystallization, and Structure Determination of the SARS-PLpro∼DiUb$^{Lys48}$-ABP Complex

The generation of recombinant SARS PLpro was described elsewhere (Békés et al., 2015), with modifications as described in Supplemental Experimental Procedures. SARS PLpro (45 μM) was reacted with diUb$^{Lys48}$-PRG (45 μM) for 30 min at 37°C in 20 mM Tris (pH 8.0), 150 mM NaCl, and 5 mM DTT; purified by size-exclusion chromatography; concentrated to 11 mg/ml; and frozen in liquid nitrogen for storage (−80°C). Diffraction-quality crystals (∼50–100 μm) grew for 1 month at 12°C by hanging drop vapor diffusion against 0.1 M MES (2-(N-morpholino)-ethanesulfonic acid) (pH 5.5), 0.1 M lithium-acetate, and 12%–20% PEGs 4000/6000/8000. Single crystals were cryo-protected by addition of 20% ethylene glycol and flash cooled in liquid nitrogen. Diffraction data were collected from a single crystal and processed, and the structure was determined using methods reported in Supplemental Experimental Procedures.

### Ub-ABP Labeling Assays

For qualitative assays, DUBs (1 μM) were incubated with excess activity-based probes (2–5 μM, monoUb-PRG, diUb$^{Lys48}$-VME ["in-between" diUb-ABP]; Mulder et al., 2014) or diUb$^{Lys48}$-PRG ("distal" diUb-ABP; Flierman et al., 2016) for indicated times at 37°C in 20 mM Tris (pH 8.0), 150 mM NaCl, and 5 mM DTT. Reactions were performed at least in duplicate. For linkage-specific distal diUb-ABPs, TAMRA-labeled probes were used in a 30-s labeling assay at 37°C. Reactions were quenched with loading sample buffer (4× LDS [Invitrogen], with 5 mM DTT), and analyzed by SDS-PAGE and SYPRO-staining. Gels were scanned to visualize the TAMRA-label (488 nM), imaged using Bio-Rad Gel-Doc, quantified by ImageJ software, and graphed with Prism. Error bars represent ±SEM.

### Kinetic Assays with -AMC Substrates

To determine apparent $k_{cat}/K_M$ for SARS PLpro and its mutants, monoUb-AMC, diUb$^{Lys48}$-AMC, and ISG15-AMC were prepared as 2-fold serial dilutions (starting at 30 μM: monoUb and diUb$^{Lys48}$ [triazole-linked]; at 15 μM: ISG15-AMC) in 20 mM Tris (pH 8.0), 150 mM NaCl, and 5 mM DTT. SARS PLpro was used at 10 nM (diUb$^{Lys48}$- and ISG15-AMC) or 50 nM (monoUb-AMC), and the final reaction volume was 10 μl. Substrates and DUBs were pre-incubated at 25°C for 1 min, and cleavage of UBL-AMCs was performed at 30°C using a Spectramax fluorescence plate reader running SoftMax Pro 5 (Molecular Devices) operated in kinetic mode in black, round-bottom 384-well plates (Corning, #3698). AMC fluorescence was monitored by excitation at 355 nm and emission at 460 nm over time for 5–10 min. Initial linear cleavage rates ($V_i$) were fitted by the Michaelis-Menten equation by Prism based on a free AMC standard curve. Experiments were performed at least in triplicate, and error bars indicate ±SEM. To compare triazole-linked or native diUb$^{Lys48}$-AMC, substrates were prepared as 2-fold serial dilutions of 3.75 μM (limited by the concentration of the native diUb$^{Lys48}$-AMC). Assays were performed in duplicate. To compare individual SARS PLpro mutants, monoUb-AMC, diUb$^{Lys48}$-AMC, and ISG15-AMC were used at 400 nM final concentrations, using 10 or 50 nM SARS PLpro. Data were plotted as percent of WT cleavage rates for each substrate (n = 3), and error bars indicate ±SEM. To compare linkage-specific diUb-AMC substrates using SARS PLpro, diUb-AMC substrates were used at 200 nM final concentrations, using 5 nM SARS PLpro. Data were plotted as percent of the diUb$^{Lys48}$-AMC cleavage rate (n = 3), and error bars indicate ±SEM.

### Gel-Based Ub Chain Cleavage Assays

Ub chains (1 μM; 20 mM Tris [pH 8.0], 150 mM NaCl, and 5 mM DTT) were cleaved at 37°C for indicated times by SARS PLpro WT and its mutants at 10 nM for penta-, tetra-, and triUb$^{Lys48}$ or 50 nM of diUb$^{Lys48}$ cleavage. Reactions were quenched with loading sample buffer (4× LDS, Invitrogen) and analyzed by SDS-PAGE and SYPRO-staining. Gels imaged using a Bio-Rad Gel-Doc, quantified by ImageJ, cropped where indicated by heavy dashed lines, and graphed using Prism. Assays using SARS mutants were performed in batches; mutants were always compared to cleavage by WT. Loss of uncleaved substrate is expressed as a percent value of uncleaved substrate over the total Ub signal per lane. Initial cleavage rates were calculated from linear portions of curves showing loss of uncleaved substrate over time and expressed as percent of WT rates in arbitrary units. Reactions performed at least in duplicate. Error bars represent ±SEM.

### DUB Assay in Lysates

Lysates from human interferon beta (IFN-β; 500 U/ml, 48 hr) or TNF-α (10 ng/ml, 10 min) and MG132 (10 μM, 40 min) stimulated HeLa cells (10 μg total lysate per reaction) were incubated with 100 or 50 nM DUBs, as indicated, in 20-μl reaction volumes with 25 mM DTT for indicated times. Reactions terminated by heating in SDS loading buffer, analyzed by SDS-PAGE and western blotting with indicated antibodies. Blots developed by horseradish peroxidase (HRP) chemiluminescence. Films were scanned, cropped where indicated by heavy dashed lines, quantified and graphed as described above. Light dashed lines in all figures included for clarity.

## ACCESSION NUMBERS

The accession number for the coordinates and structure factors reported in this paper is PDB: 5E6J.

## SUPPLEMENTAL INFORMATION

Supplemental Information includes Supplemental Experimental Procedures and six figures and can be found with this article online at http://dx.doi.org/10.1016/j.molcel.2016.04.016.

## AUTHOR CONTRIBUTIONS

M.B. initiated and performed the study with guidance from T.T.H. and C.D.L. G.J.v.d.H.v.N. synthesized diUb$^{LysX}$-AMC substrates and biotin-triUb$^{Lys48}$; R.E. synthesized distal diUb$^{LysX}$-ABP probes in H.O.'s laboratory. M.B. and C.D.L. determined the structure and wrote the manuscript.

## ACKNOWLEDGMENTS

The authors thank members of the T.T.H., C.D.L., and H.O. labs for reagents and discussions, particularly E. Wasmuth and L. Cappadocia for assistance in crystallography. NE-CAT beamlines are funded by the National Institutes of Health (NIH) National Institute of General Medical Sciences (NIGMS) (P41 GM103403) and the Advanced Photon Source is operated for the Department of Energy Office of Science by Argonne National Laboratory under contract DE-AC02-06CH11357. This work was supported in part by NIH/NIGMS F32GM100598 (M.B.), GM084244 and ES025166 (T.T.H.), GM065872 (C.D.L.), NIH National Cancer Institute P30 CA008748 (Sloan Kettering), NYU Laura & Isaac Perlmutter Cancer Center Support Grant's Developmental Project Program P30 CA016087 (T.T.H.), NWO-VENI grant 722.014.002 (G.v.d.H.v.N), NOW-VICI grant 724.013.002 (H.O.), and ERC grant agreement number 281699 (H.O.). C.D.L. is an investigator of the Howard Hughes Medical Institute. The content is solely the responsibility of the authors and does not represent the official views of the NIH. M.B., T.T.H, C.D.L., R.E., and G.J.v.d.H.v.N. declare no competing financial interests. H.O. is part of the DUB Alliance that includes Cancer Research Technology and FORMA Therapeutics and is a founder and stakeholder of UbiQ, which holds intellectual property rights to technology for reagent generation.

Received: October 21, 2015
Revised: March 14, 2016
Accepted: April 15, 2016
Published: May 19, 2016

## REFERENCES

Báez-Santos, Y.M., Mielech, A.M., Deng, X., Baker, S., and Mesecar, A.D. (2014). Catalytic function and substrate specificity of the papain-like protease domain of nsp3 from the Middle East respiratory syndrome coronavirus. J. Virol. *88*, 12511–12527.

Bailey-Elkin, B.A., Knaap, R.C., Johnson, G.G., Dalebout, T.J., Ninaber, D.K., van Kasteren, P.B., Bredenbeek, P.J., Snijder, E.J., Kikkert, M., and Mark, B.L. (2014a). Crystal structure of the Middle East respiratory syndrome coronavirus (MERS-CoV) papain-like protease bound to ubiquitin facilitates targeted disruption of deubiquitinating activity to demonstrate its role in innate immune suppression. J. Biol. Chem. *289*, 34667–34682.

Bailey-Elkin, B.A., van Kasteren, P.B., Snijder, E.J., Kikkert, M., and Mark, B.L. (2014b). Viral OTU deubiquitinases: a structural and functional comparison. PLoS Pathog. *10*, e1003894.

Békés, M., Rut, W., Kasperkiewicz, P., Mulder, M.P., Ovaa, H., Drag, M., Lima, C.D., and Huang, T.T. (2015). SARS hCoV papain-like protease is a unique Lys48 linkage-specific di-distributive deubiquitinating enzyme. Biochem. J. *468*, 215–226.

Berger, A., and Schechter, I. (1970). Mapping the active site of papain with the aid of peptide substrates and inhibitors. Philos. Trans. R. Soc. Lond. B Biol. Sci. *257*, 249–264.

Bhoj, V.G., and Chen, Z.J. (2009). Ubiquitylation in innate and adaptive immunity. Nature *458*, 430–437.

Bogunovic, D., Byun, M., Durfee, L.A., Abhyankar, A., Sanal, O., Mansouri, D., Salem, S., Radovanovic, I., Grant, A.V., Adimi, P., et al. (2012). Mycobacterial disease and impaired IFN-γ immunity in humans with inherited ISG15 deficiency. Science *337*, 1684–1688.

Capodagli, G.C., McKercher, M.A., Baker, E.A., Masters, E.M., Brunzelle, J.S., and Pegan, S.D. (2011). Structural analysis of a viral ovarian tumor domain protease from the Crimean-Congo hemorrhagic fever virus in complex with covalently bonded ubiquitin. J. Virol. *85*, 3621–3630.

Cer, R.Z., Mudunuri, U., Stephens, R., and Lebeda, F.J. (2009). IC50-to-Ki: a web-based tool for converting IC50 to Ki values for inhibitors of enzyme activity and ligand binding. Nucleic Acids Res. *37*, W441–W445.

Channappanavar, R., Fehr, A.R., Vijay, R., Mack, M., Zhao, J., Meyerholz, D.K., and Perlman, S. (2016). Dysregulated Type I Interferon and Inflammatory Monocyte-Macrophage Responses Cause Lethal Pneumonia in SARS-CoV-Infected Mice. Cell Host Microbe *19*, 181–193.

Chau, V., Tobias, J.W., Bachmair, A., Marriott, D., Ecker, D.J., Gonda, D.K., and Varshavsky, A. (1989). A multiubiquitin chain is confined to specific lysine in a targeted short-lived protein. Science *243*, 1576–1583.

Clague, M.J., Liu, H., and Urbé, S. (2012). Governance of endocytic trafficking and signaling by reversible ubiquitylation. Dev. Cell *23*, 457–467.

Cook, W.J., Jeffrey, L.C., Carson, M., Chen, Z., and Pickart, C.M. (1992). Structure of a diubiquitin conjugate and a model for interaction with ubiquitin conjugating enzyme (E2). J. Biol. Chem. *267*, 16467–16471.

Ekkebus, R., van Kasteren, S.I., Kulathu, Y., Scholten, A., Berlin, I., Geurink, P.P., de Jong, A., Goerdayal, S., Neefjes, J., Heck, A.J., et al. (2013). On terminal alkynes that can react with active-site cysteine nucleophiles in proteases. J. Am. Chem. Soc. *135*, 2867–2870.

El Oualid, F., Merkx, R., Ekkebus, R., Hameed, D.S., Smit, J.J., de Jong, A., Hilkmann, H., Sixma, T.K., and Ovaa, H. (2010). Chemical synthesis of ubiquitin, ubiquitin-based probes, and diubiquitin. Angew. Chem. Int. Ed. Engl. *49*, 10149–10153.

Flierman, D., van Noort, G.J.v.d.H.v., Ekkebus, R., Gerink, P.P., Mevissen, T.E.T., Hospenthal, M.K., Komander, D., and Ovaa, H. (2016). Non-hydrolyzable diubiquitin probes reveal linkage-specific reactivity of deubiquitylating enzymes mediated by s2 pockets. Cell Chem. Biol., Published online April 6, 2016. http://dx.doi.org/10.1016/j.chembiol.2016.03.009.

Fushman, D., and Wilkinson, K.D. (2011). Structure and recognition of polyubiquitin chains of different lengths and linkage. F1000 Biol. Rep. *3*, 26.

Hemelaar, J., Borodovsky, A., Kessler, B.M., Reverter, D., Cook, J., Kolli, N., Gan-Erdene, T., Wilkinson, K.D., Gill, G., Lima, C.D., et al. (2004). Specific and covalent targeting of conjugating and deconjugating enzymes of ubiquitin-like proteins. Mol. Cell. Biol. *24*, 84–95.

Isaacson, M.K., and Ploegh, H.L. (2009). Ubiquitination, ubiquitin-like modifiers, and deubiquitination in viral infection. Cell Host Microbe *5*, 559–570.

Keusekotten, K., Elliott, P.R., Glockner, L., Fiil, B.K., Damgaard, R.B., Kulathu, Y., Wauer, T., Hospenthal, M.K., Gyrd-Hansen, M., Krappmann, D., et al. (2013). OTULIN antagonizes LUBAC signaling by specifically hydrolyzing Met1-linked polyubiquitin. Cell *153*, 1312–1326.

Kirkpatrick, D.S., Hathaway, N.A., Hanna, J., Elsasser, S., Rush, J., Finley, D., King, R.W., and Gygi, S.P. (2006). Quantitative analysis of in vitro ubiquitinated cyclin B1 reveals complex chain topology. Nat. Cell Biol. *8*, 700–710.

Komander, D., and Rape, M. (2012). The ubiquitin code. Annu. Rev. Biochem. *81*, 203–229.

Komander, D., Reyes-Turcu, F., Licchesi, J.D., Odenwaelder, P., Wilkinson, K.D., and Barford, D. (2009). Molecular discrimination of structurally equivalent Lys 63-linked and linear polyubiquitin chains. EMBO Rep. *10*, 466–473.

Lindner, H.A., Lytvyn, V., Qi, H., Lachance, P., Ziomek, E., and Ménard, R. (2007). Selectivity in ISG15 and ubiquitin recognition by the SARS coronavirus papain-like protease. Arch. Biochem. Biophys. *466*, 8–14.

Mevissen, T.E., Hospenthal, M.K., Geurink, P.P., Elliott, P.R., Akutsu, M., Arnaudo, N., Ekkebus, R., Kulathu, Y., Wauer, T., El Oualid, F., et al. (2013). OTU deubiquitinases reveal mechanisms of linkage specificity and enable ubiquitin chain restriction analysis. Cell *154*, 169–184.

Mielech, A.M., Chen, Y., Mesecar, A.D., and Baker, S.C. (2014). Nidovirus papain-like proteases: multifunctional enzymes with protease, deubiquitinating and deISGylating activities. Virus Res. *194*, 184–190.

Mulder, M.P., El Oualid, F., ter Beek, J., and Ovaa, H. (2014). A native chemical ligation handle that enables the synthesis of advanced activity-based probes: diubiquitin as a case study. ChemBioChem *15*, 946–949.

Narasimhan, J., Wang, M., Fu, Z., Klein, J.M., Haas, A.L., and Kim, J.J. (2005). Crystal structure of the interferon-induced ubiquitin-like protein ISG15. J. Biol. Chem. *280*, 27356–27365.

Pickart, C.M. (2001). Mechanisms underlying ubiquitination. Annu. Rev. Biochem. *70*, 503–533.

Ratia, K., Saikatendu, K.S., Santarsiero, B.D., Barretto, N., Baker, S.C., Stevens, R.C., and Mesecar, A.D. (2006). Severe acute respiratory syndrome coronavirus papain-like protease: structure of a viral deubiquitinating enzyme. Proc. Natl. Acad. Sci. USA *103*, 5717–5722.

Ratia, K., Kilianski, A., Baez-Santos, Y.M., Baker, S.C., and Mesecar, A. (2014). Structural Basis for the Ubiquitin-Linkage Specificity and deISGylating activity of SARS-CoV papain-like protease. PLoS Pathog. *10*, e1004113.

Reyes-Turcu, F.E., Ventii, K.H., and Wilkinson, K.D. (2009). Regulation and cellular roles of ubiquitin-specific deubiquitinating enzymes. Annu. Rev. Biochem. *78*, 363–397.

Sato, Y., Yoshikawa, A., Yamagata, A., Mimura, H., Yamashita, M., Ookata, K., Nureki, O., Iwai, K., Komada, M., and Fukai, S. (2008). Structural basis for specific cleavage of Lys 63-linked polyubiquitin chains. Nature *455*, 358–362.

Sato, Y., Goto, E., Shibata, Y., Kubota, Y., Yamagata, A., Goto-Ito, S., Kubota, K., Inoue, J., Takekawa, M., Tokunaga, F., and Fukai, S. (2015). Structures of CYLD USP with Met1- or Lys63-linked diubiquitin reveal mechanisms for dual specificity. Nat. Struct. Mol. Biol. *22*, 222–229.

Totura, A.L., and Baric, R.S. (2012). SARS coronavirus pathogenesis: host innate immune responses and viral antagonism of interferon. Curr. Opin. Virol. *2*, 264–275.

Ye, Y., Blaser, G., Horrocks, M.H., Ruedas-Rama, M.J., Ibrahim, S., Zhukov, A.A., Orte, A., Klenerman, D., Jackson, S.E., and Komander, D. (2012). Ubiquitin chain conformation regulates recognition and activity of interacting proteins. Nature *492*, 266–270.

Zhang, X., Bogunovic, D., Payelle-Brogard, B., Francois-Newton, V., Speer, S.D., Yuan, C., Volpi, S., Li, Z., Sanal, O., Mansouri, D., et al. (2015). Human intracellular ISG15 prevents interferon-α/β over-amplification and auto-inflammation. Nature *517*, 89–93.

**Molecular Cell, Volume *62***

## Supplemental Information

# Recognition of Lys48-Linked Di-ubiquitin and Deubiquitinating Activities of the SARS Coronavirus Papain-like Protease

**Miklós Békés, Gerbrand J. van der Heden van Noort, Reggy Ekkebus, Huib Ovaa, Tony T. Huang, and Christopher D. Lima**

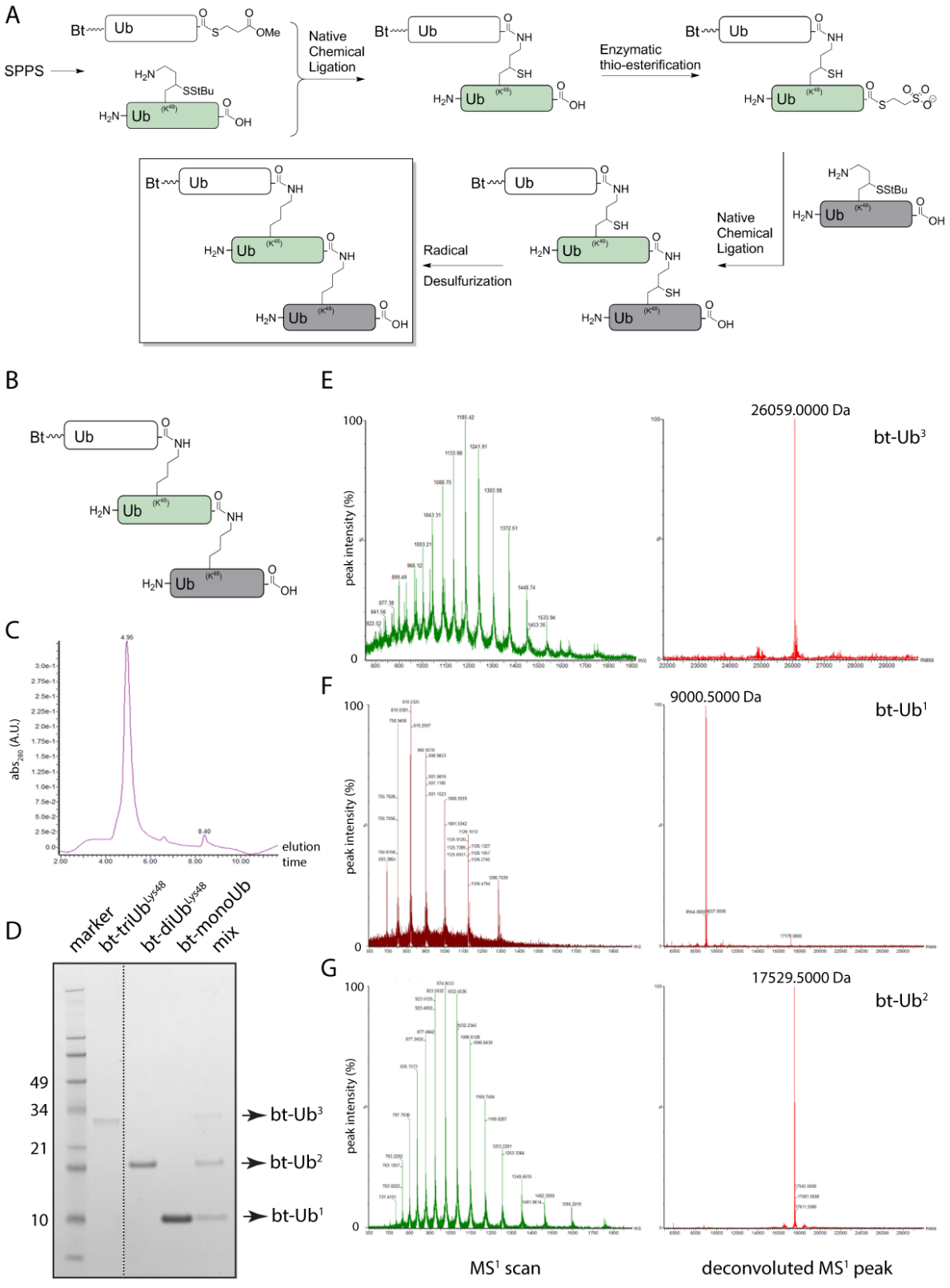


**Figure S1 – related to Figure 1**

A) Detailed synthesis scheme to obtain the native tri-ubiquitin$^{Lys48}$ substrate carrying a single biotin tag on the N-terminus of the distal ubiquitin moiety. B) Schematics of the final biotin-triUb$^{Lys48}$ substrate. C) LC-MS chromatography UV-profile of the final bt-triUb$^{Lys48}$ product. D) Coommassie-stained SDS-PAGE analysis of the final bt-triUb$^{Lys48}$ substrate, along with biotin-tagged mono- and diUb$^{Lys48}$ controls. E-G) MS$^1$ analysis (on the left) and deconvoluted mass spectra (on the right) of bt-triUb$^{Lys48}$ (E), bt-monoUb (F), and bt-diUb$^{Lys48}$ (G).

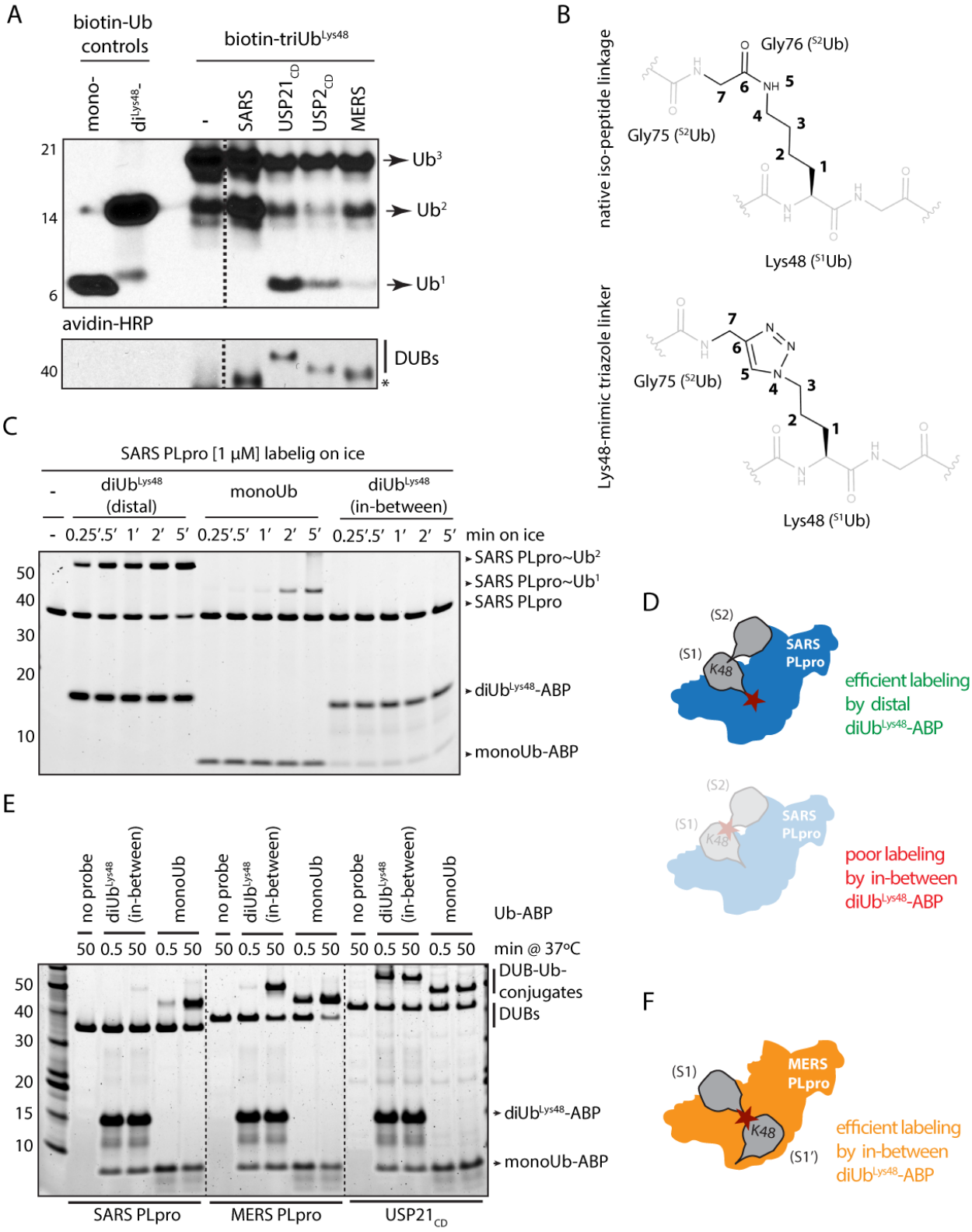


**Figure S2 – related to Figure 1**

A) Cleavage of biotin-triUb$^{Lys48}$ by various DUBs [100 nM] for 15 min at 37ºC. Notice that the biotin-tag can be visualized on both mono- and diUb products for USP21$_{CD}$, UPS2$_{CD}$ and MERS PLpro, while it remains visible only on the diUb$^{Lys48}$ product for SARS PLpro. B) Comparison of the chemical structure of a native isopeptide-bond (top) and the isosteric triazole linkage used in the distal diUb$^{Lys48}$-ABP (bottom). The number of atoms between the main-chain C-α of Lys48 of $^{S1}$Ub and the main chain nitrogen of Gly75 of $^{S2}$Ub is shown in bold, indicating similar distance and geometry of the triazole mimic. C) Representative gels of quantitative labeling assays of SARS PLpro by Ub-ABPs on ice used to generate Figure 1F. D) Schematics of SARS PLpro labeling by diUb-ABPs. E) Qualitative labeling assay of USP-family DUBs by the in-between diUb$^{Lys48}$-ABP. F) Schematics of diUb-ABP labeling for the related MERS PLpro, a monoUb-based DUB.

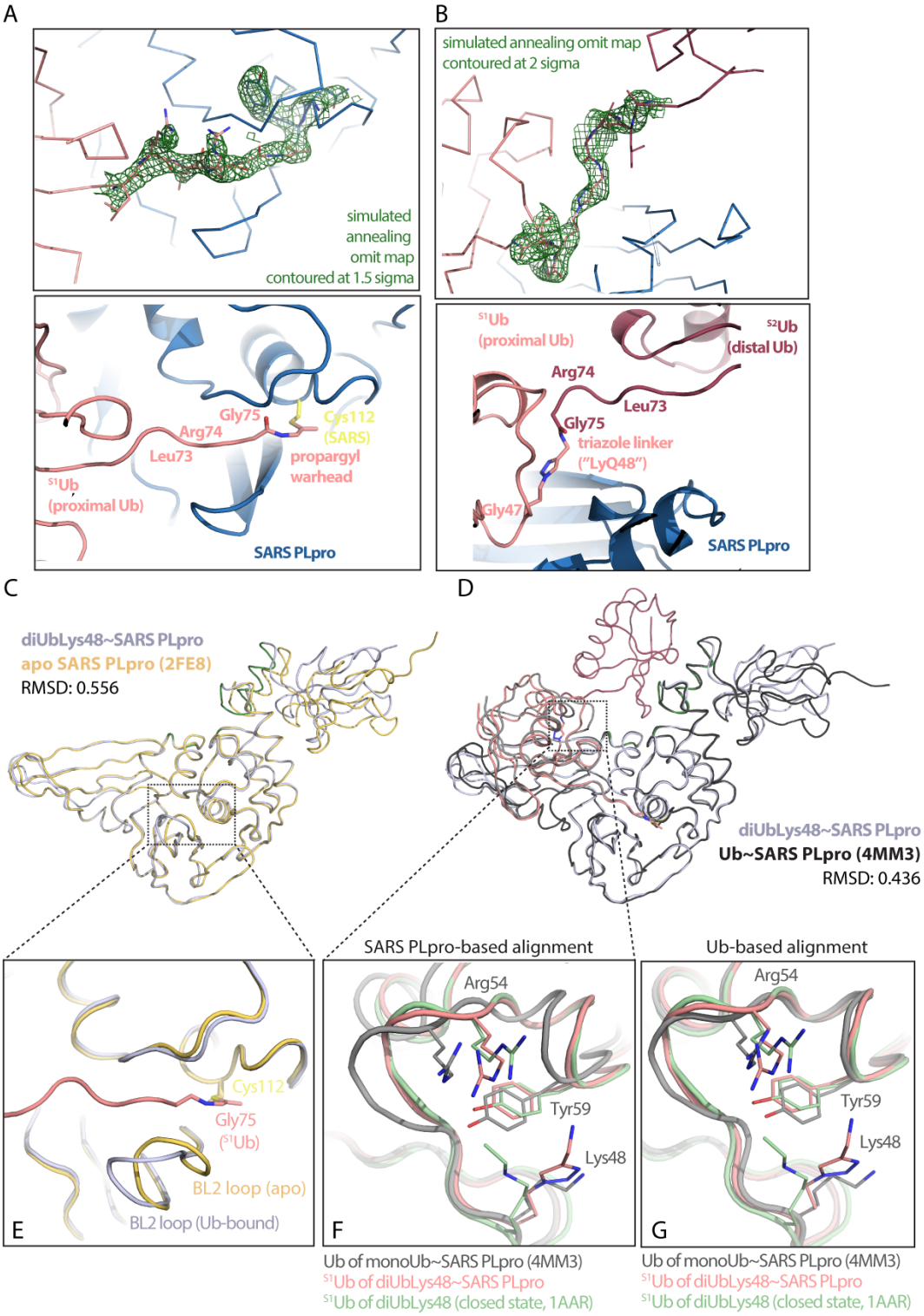


**Figure S3 – related to Figure 2**

A) Simulated annealing omit map contoured at 1.5σ (top) and cartoon representation (bottom) of the covalent linkage by the propargyl warhead between $^{S1}$Ub-Gly75 and SARS-PLpro-Cys112. B) Simulated annealing omit map contoured at 2σ (top) and cartoon representation (bottom) of the covalent linkage by the triazole linker between $^{S2}$Ub-Gly75 and $^{S1}$Ub-Lys48. C) Cartoon representation of the structure-based alignment of SARS PLpro from the diUb$^{Lys48}$ complex (in blue-white) and the apo SARS PLpro structure (PDB 2FE8, in wheat (Ratia et al., 2006)). D) Structure-based alignment of SARS PLpro from the diUb$^{Lys48}$ complex (in blue-white) and from the monoUb-aldehyde complex (PDB 4MM3, SARS in black, Ub in grey (Ratia et al., 2014)). E) Detail of the alignment in C), showing orientation of the BL2 loop. E-G) Structure-based alignment of the diUb$^{Lys48}$-SARS complex with free diUb$^{Lys48}$ (PDB 1AAR (Cook et al., 1992)) and the SARS monoUb complex (4MM3). In F), alignment was performed based on the SARS DUB domain; in G) alignment was performed based on the proximal Ub.

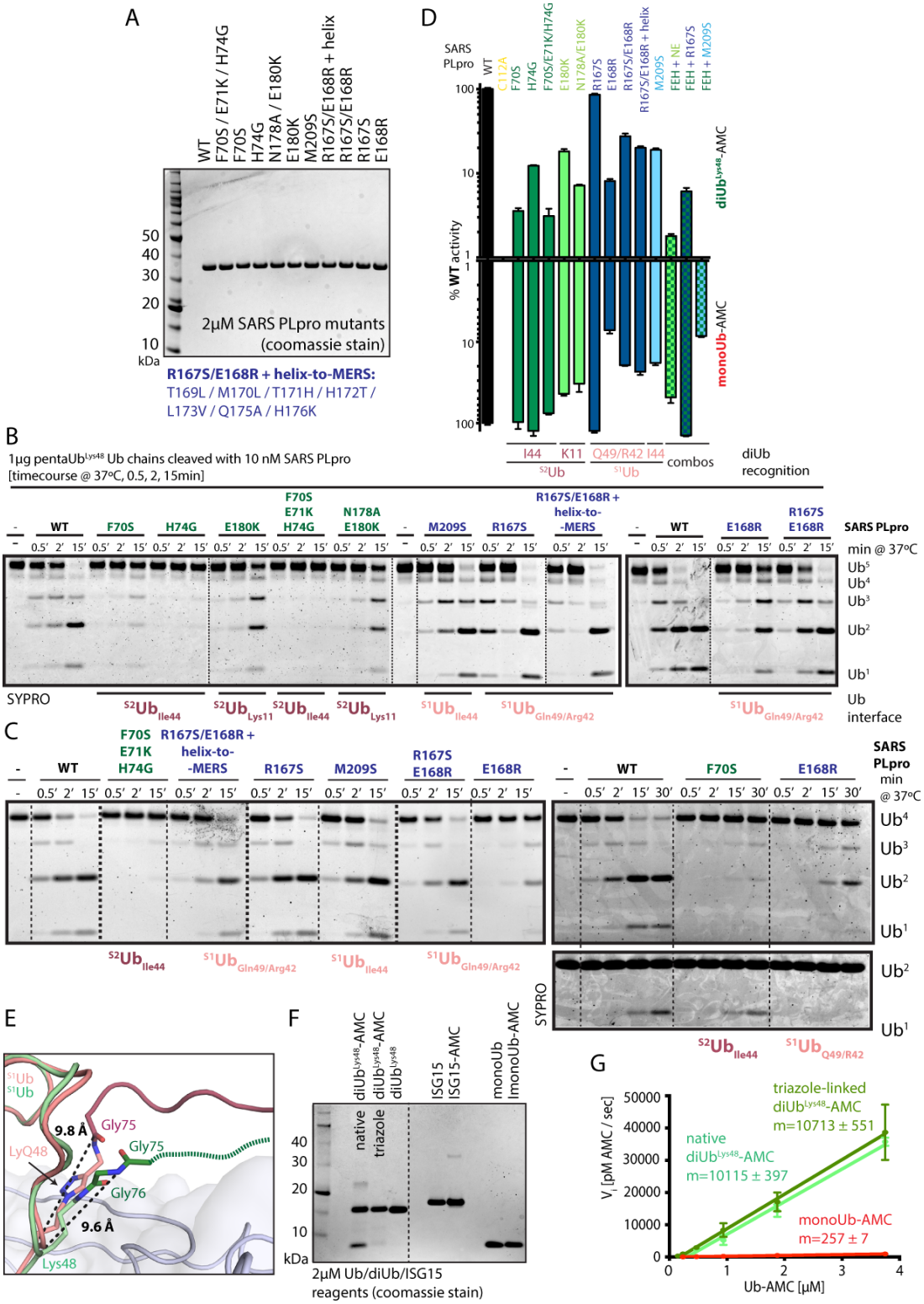


**Figure S4 – related to Figure 3**

A) Purified SARS PLpro mutants (2 μM) analyzed by SDS-PAGE and coomassie staining. B) Representative gels used to monitor pentaUb$^{Lys48}$ cleavage activity of SARS PLpro mutants shown in Figure 3A. Dotted lines indicate cropping between gels. C) Qualitative cleavage assay of tetra- and diUb$^{Lys48}$ by 10 nM and 50nM SARS PLpro mutants, respectively. Light dotted lines are included for clarity; heavy dotted lines indicate cropping between gels. D) Initial cleavage of SARS PLpro WT (in black), its $^{S2}$Ub (in green), its $^{S1}$Ub (in blue) and combination mutants on diUb$^{Lys48}$-AMC (top panel, triazole-linked) and monoUb-AMC (bottom panel) substrates, expressed as percent of WT activity. Error bars represent ±SEM. E) Structure-based alignment of the diUb$^{Lys48}$-SARS complex with free diUb$^{Lys48}$ (PDB 1AAR), showing the geometry and distance of the triazole-linker compared to the native isopeptide-linkage. F) Coomassie gel of Ub-reagents used in this study for kinetic and inhibition analysis, which is shown in Table 2. G) Initial cleavage rates of triazole-linked (dark green line) and native (light green line) diUb$^{Lys48}$-AMC substrates by SARS PLpro.

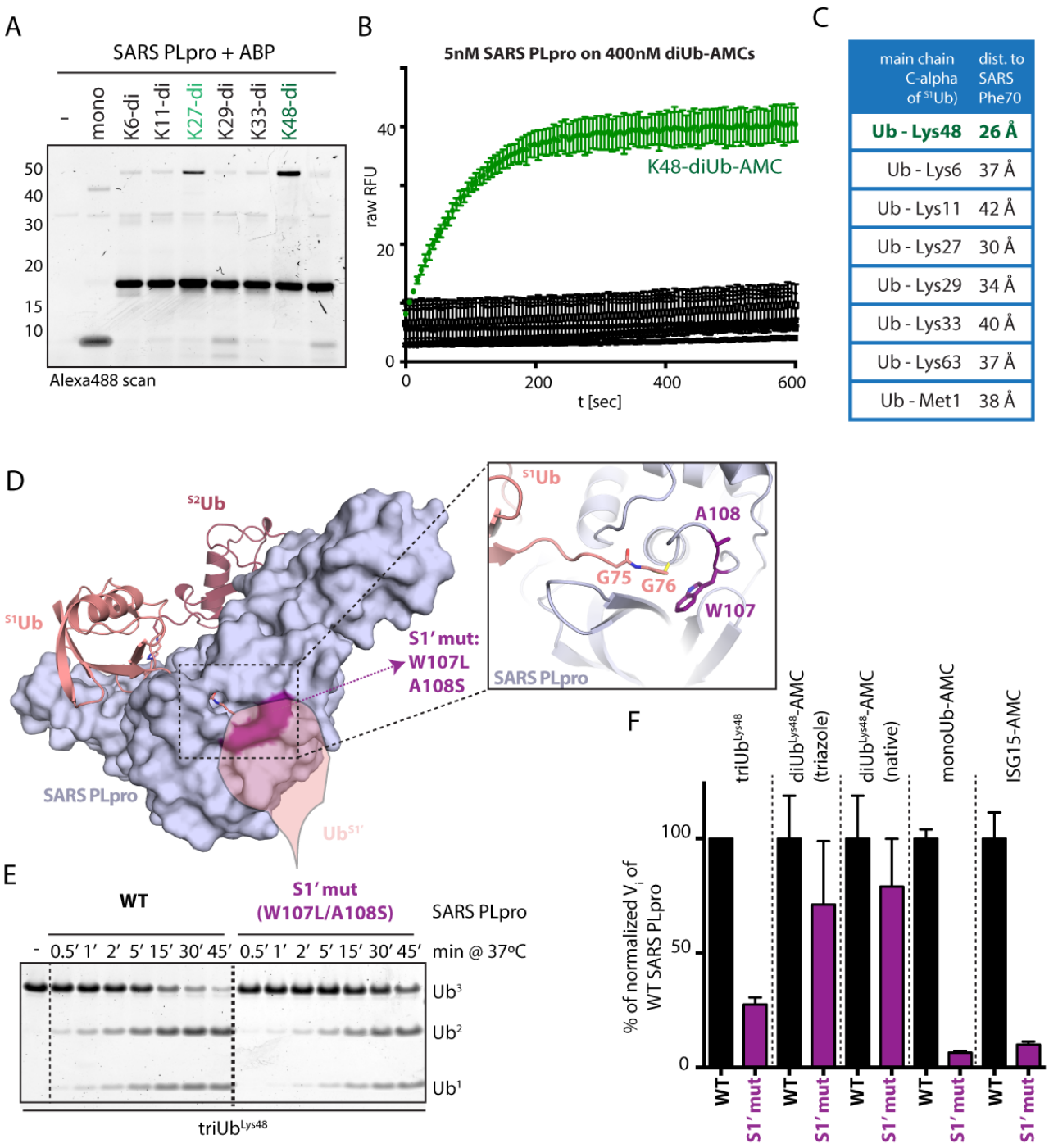


**Figure S5 – related to Figure 4**

A) Labeling assay of SARS PLpro with linkage-specific diUb-ABPs at 37ºC for 30 sec (as shown in Figure 4A), visualized by Alexa488-scan (at 488 nm) to reveal the diUb probes. B) Example raw relative fluorescence unit (RFU) progress curves for linkage-specific diUb-AMC substrate cleavage reactions. Triplicates of such reactions were used to generate Figure 4B; in green is the diUb$^{Lys48}$-AMC; in black are all other -AMC substrates. C) Distances (in Å) between the main-chain C-α of each Ub chain forming residue of $^{S1}$Ub to Phe70 of the $^{S2}$Ub binding site in SARS PLpro. D) Structure-based representation of a putative S1' mutant – W107L/A108S – shown in purple; the inset shows a zoom for the active site of SARS PLpro, Trp107 and Ala108 are shown as sticks. E) Gel-based cleavage assay of 10nM SARS PLpro WT versus the W107L/A108S mutant. Initial cleavage rates are quantified in Supplementary Figure 5F (first panel). F) TriUb$^{Lys48}$ cleavage rates (from Supplementary Figure 5E) expressed as percent of WT, compared to cleavage rates of WT and the W107L/A108S mutant on triazole-linked and native diUb$^{Lys48}$-, monoUb- and ISG15-AMC substrates Error bars represent ±SEM, n=2 for triUb$^{Lys48}$, n=4 for monoUb-, diUb$^{Lys48}$(native and triazole-linked)- and ISG15-AMC substrates.

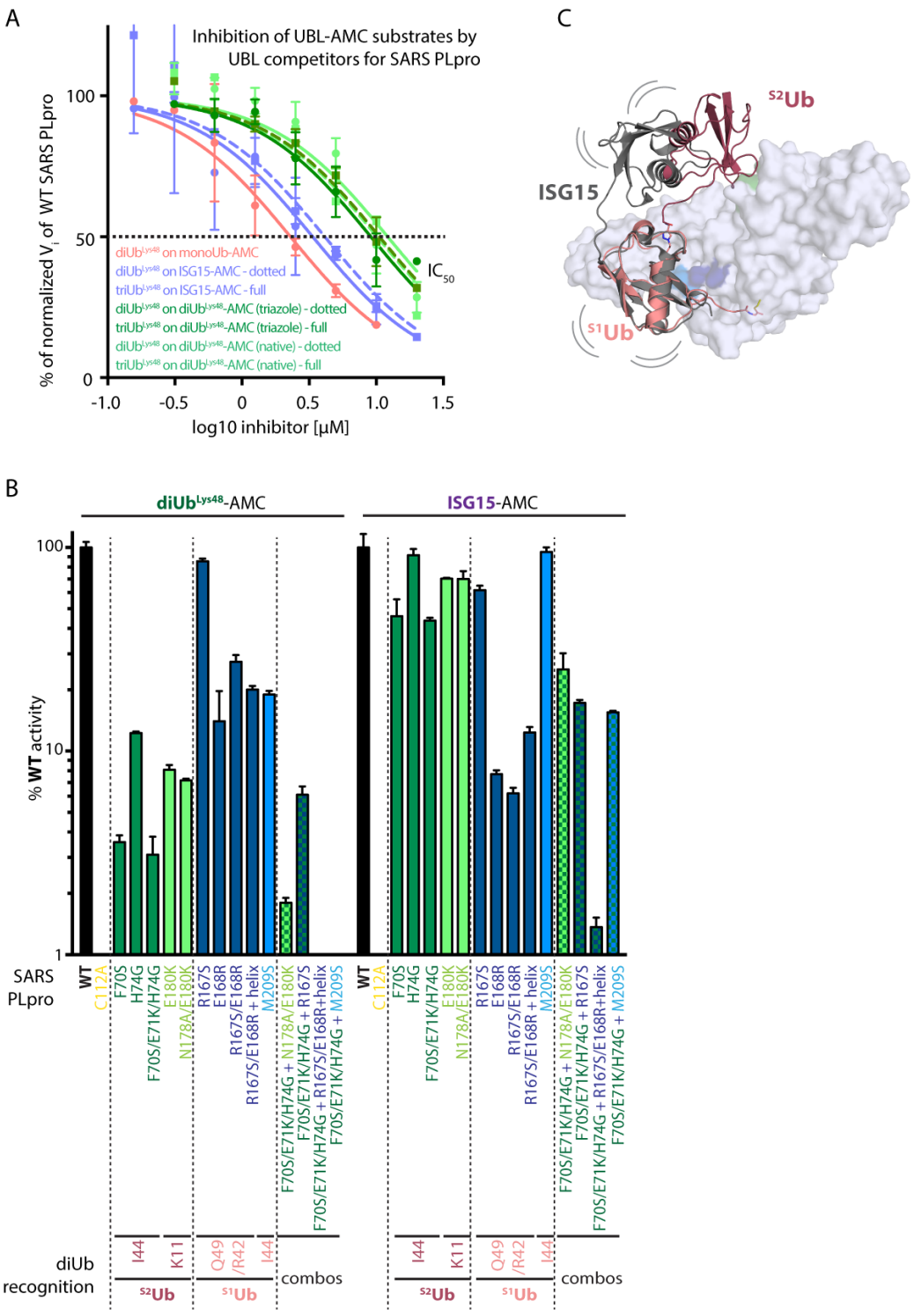


**Figure S6 – related to Figure 5 and Table 2**

A) Inhibition assays of Ub-based inhibitors on Ubl-AMC substrates graphed as $IC_{50}$ values, showing percent of no inhibitor cleavage rates at each inhibitor concentration. $IC_{50}$ values were transformed into $K_i$ values (Cer et al., 2009) and are shown in Table 2. Dark green full line – $diUb^{Lys48}$ on $diUb^{Lys48}$-AMC (triazole-linked); dark green dotted line – $triUb^{Lys48}$ on $diUb^{Lys48}$-AMC (triazole-linked); light green full line – $diUb^{Lys48}$ on $diUb^{Lys48}$-AMC (native); light green dotted line – $triUb^{Lys48}$ on $diUb^{Lys48}$-AMC (native); purple full line – $diUb^{Lys48}$ on ISG15-; purple dotted line – $triUb^{Lys48}$ on ISG15-AMC; pink full line – $diUb^{Lys48}$ on monoUb-AMC. B) Activity of SARS PLpro and its mutants on ISG15-AMC hydrolysis (compared to $diUb^{Lys48}$-AMC, data for $diUb^{Lys48}$-AMC are taken from Supplemental Figure 4D). C) Modeling of ISG15 (in grey, PDB 1Z2M) bound to SARS PLpro by aligning its proximal Ub-like domain to $^{S1}$Ub in the SARS-PLpro~$diUb^{Lys48}$ complex. Curved lines indicate the presumed flexibility of the ISG15. Dotted lines are included for clarity. Error bars represent ±SEM.

## SUPPLEMENTAL EXPERIMENTAL PROCEDURES

### Synthesis of the singly-biotinylated triUb$^{Lys48}$ substrate

The singly biotin-tagged triUb$^{Lys48}$ chain substrate was generated using a combination of native chemical ligation reactions, enzymatic thio-esterification and radical desulfurization on synthetically produced Ub thio-ester- and thiolysine-mutants (Merkx et al., 2013). Briefly, synthetic N-terminally biotinylated Ub thioester (25 mg/mL) and synthetic K48-thiolysine Ub (25 mg/mL) were ligated in 8 M Gdn.HCl / 200 mM $NaH_2PO_4$, pH 7.6 in the presence of 1.2 M mercaptophenyl acetic acid (MPAA) for 16 hours at 37$^o$C. After HPLC and size exclusion chromatography (SEC), the resulting Bt-diUb$^{Lys48}$ C-terminal carboxylic acid (13 mg/mL) was converted to its MESNa-thioester using recombinant UBA-E1 ubiquitin activating enzyme (250 nM) in 200 mM HEPES buffer, pH 7.7 containing 10 mM ATP, 10 mM $MgCl_2$ and 100 mM MESNa for 1 hour at 37$^o$C. After HPLC purification, the appropriate fractions were pooled and lyophilized to yield Bt-diUb$^{Lys48}$-MESNa, which was ligated to K48-thiolysine Ub (25 mg/mL) in 8 M Gdn.HCl/ 200 mM $NaH_2PO_4$, pH 7.6 in the presence of 1.2 M MPAA for 16 hours at 37$^o$C. After HPLC- and Size Exclusion Chromatography the resulting Bt-Ub$_3^{Lys48}$ was desulfurized in 8 M Gdn.HCl/200 mM $NaH_2PO_4$, pH 6.8 in the presence of 200 mM TCEP, 75 mM GSH (reduced form) and 75 mM of the radical initiator VA-044. Concomitant HPLC and subsequent SEC-purification resulted in the target compound: Bt-triUb$^{Lys48}$

### Cloning, protein expression, purification and crystallization.

The generation of recombinant SARS and MERS PLpro has been previously described (Bekes et al., 2015). Briefly, the nucleotide sequence (nts 4451-7179) from MERS HCoV ORF1a (GenBank AGV08402.1) and the nucleotide sequence encoding the SARS PLpro minimal domain (nts 4884-5829, aa 1541-1885, PDB: 3MJ5) were gene synthesized by GenScript and subcloned into pET28b with a C-terminal 6xHis-tag. All mutations were generated by over-lapping PCR and verified by sequencing. DUBs (SARS and MERS PLpro and USP21$_{CD}$) were expressed in *E.coli* BL-21 codon plus RIL cells and purified until homogeneity as previously (Bekes et al., 2015). Briefly, *E.coli* was grown at 37ºC until $OD_{600}$=1.0 and induced with 1 mM IPTG and further incubated at 30ºC for 4 hours. Harvested cell pellets were flash frozen in liquid nitrogen and stored at -80ºC until purification. Frozen pellets were thawed on ice and lysed in 20 mM Tris, pH=8.0, 350 mM NaCl, 1 mM PMSF, 1 mM beta-mercaptoethanol, 1% NP-40 and 10 mM imidazole by sonication. After centrifugation, the supernatant was applied onto Ni-NTA resin (Quiagen) for batch-binding by rotation for 1 hour at 4ºC. Ni-bound DUBs were eluted with 20 mM Tris, pH=8.0, 350 mM NaCl, 250 mM imidazole and 1 mM beta-mercaptoethanol, concentrated and purified by size-exclusion chromatography on a Superdex-75 (16/600) column (GE); peak fractions were collected, concentrated to 1-10 mg/mL, aliquoted and stored at -80ºC until use. SARS PLpro mutants were purified by Ni-NTA purifications and buffer exchanged into assay buffer (20 mM Tris, pH=8.0, 150 mM NaCl using BioRad spin-columns and supplemented with 1 mM DTT prior to biochemical assays.

### Structure Determination

X-ray diffraction data were processed using HKL2000 (Otwinowski, 1997), the statistics obtained by Phenix (Adams et al., 2010) are reported in Table 1. Crystals were in space group $P2_1$ with two complexes in the asymmetric unit. An initial structure solution was obtained by molecular replacement by Phaser (McCoy et al., 2007) using coordinates of the apo form of SARS PLpro (PDB 2FE8 (Ratia et al., 2006)), monoUb-bound SARS PLpro (PDB 4MM3 (Ratia et al., 2014)) and of monoUb (PDB 1UBQ), which model then subsequently underwent iterative refinement and further modeling in Coot (Emsley et al., 2010) to add the second Ub, manually model the propargyl warhead (between $^{S1}$Ub-Gly75 and SARS PLpro-Cys112) and the triazole linkage (between $^{S1}$Ub-Lys48 and $^{S2}$Ub-Gly75) in the continuous electron density within the covalent complex. The two complexes in the ASU align with an RMS of 0.978 over 3350 atoms (SARS PLpro amino acids 4-316 and the two full-length Ub molecules). A final model with $R_{work}/R_{free}$ of 23.2/26.4 at 2.85Å resolution was obtained with good geometry, as assessed by MolProbity (Chen et al., 2010), (with 93.3%, 99.7%, and 0.3% in favored, allowed, and disallowed regions of Ramachandran space, respectively). Figures showing the structure were generated using Pymol (The PyMOL Molecular Graphics System, version 1.5.0.4. Schrödinger, LLC.) The final model has the PDB code 5E6J.

### Synthesis of mono- and diUb activity-based probes and -AMC derivative substrates with the triazole linkage

For generation and characterization of the non-hydrolyzable "distal" diUb activity-based probes and -AMC derivative substrates, please refer to the manuscript by Flierman et al. in Cell Chemical Biology (Flierman et al., 2016).

### Synthesis of diUb-AMC substrates (native linkage)

DiUb$^{Lys48}$ carrying a native isopeptide-linkage, equipped with a C-terminal 7-amido-4-methyl-coumarine (AMC) was generated using a procedure based on a previously reported native chemical ligation protocol (El Oualid et al., 2010) as described above, starting from synthetic Ub thioester and synthetic K48-thiolysine Ub-AMC.

### Biotin-triUb$^{Lys48}$ cleavage assays

In a reaction volume of 10 µL, 0.5 µg biotin-triUb$^{Lys48}$ substrate (in 20 mM Tris, pH 8.0, 150 mM NaCl and 5 mM DTT) was cleaved with 100 nM DUBs for 5 min at 37ºC or with a 1/5-serial dilution of SARS PLpro starting at 500 nM. Reactions were terminated with loading buffer (4X LDS, Invitrogen), boiled for 5min at 95ºC (the standard protocol for

SDS-PAGE) split into two and analyzed in parallel by SDS-PAGE and SYPRO-staining; and by SDS-PAGE, then transferred to PVDF membranes and incubated with streptavidin-HRP. Biotin-labeled Ub cleavage products were visualized by chemiluminescence, blots were developed by film.

**Inhibition assays using fluorogenic substrates**

To determine $IC_{50}$ values, a fixed concentration of monoUb-, $diUb^{Lys48}$-AMC or ISG15-AMC at 200 nM was mixed at 25ºC with a 2-fold serial dilution of inhibitor (starting at 15 or 30 μM), then mixed immediately with 5-50 nM SARS PLpro in a final volume of 15 μL. Inhibition assays were performed at 30ºC using a Spectramax fluorescence plate reader running SoftMax Pro 5 (Molecular Devices) operated in kinetic mode, in black, round-bottom 384-well plates (Corning #3698), where free AMC fluorescence was monitored by excitation at 355 nm and emission at 460 nm over time for 5-10 min. Initial linear cleavage rates ($V_i$) were expressed as percent of no inhibitor cleavage rate for every run and were fitted to Prism's log(inhibitor) vs. normalized curve equation, which calculated $IC_{50}$ values. $IC_{50}$ were then transformed into $K_i$ values based on the equation $K_i = IC_{50}/(S/K_M+1)$, assuming low affinity, competitive inhibition, where S is the concentration of the substrate (*Cer et al. 2009, NAR*). Kinetic and inhibition parameters are presented in Table 2.

**Commercial reagents**

Ub chains, Ub-AMC and ISG15-AMC were purchased from Boston Biochem. Antibodies used in this study were anti-ISG15 (#2743 from Cell Signaling), anti-Ub (P4D1, sc-8017 from Santa Cruz Biotech), anti-His (in-house, gift of D. Reinberg, NYUMC), anti-IκBα (C-21, Santa Cruz Biotech), and anti-K48-linkage (Apu2, Millipore). Streptavidin-HRP was purchased from GE Healthcare (#RPN123V).

**Cell culture and cell lysate preparation**

HeLa cells were cultured by standard cell culture technique, in DMEM with glutamine, penicillin/streptomycin, and 10% FBS at 37ºC with 5% $CO_2$. Cells were left untreated or treated with 500 units/mL of interferon-beta (human IFNβ1a, purchased from PBL Interferon Source, product #1141501) for 48 hours at 37ºC and the proteasome inhibitor MG132 (10 μM, Calbiochem) was included for the last 4 hours in the cell culture before harvest. For TNF-α treatments, HeLa cells were pre-treated with fresh media containing 10 μM MG132 for 30 min at 37ºC, then 10 ng/mL TNF-α was added directly to the media and cells were incubated for another 15 min at 37ºC. Cells were immediately harvested by scraping in cold PBS and pellets were frozen at -80ºC. Pellets were lysed on ice for 1 hour in 50 mM Tris, pH=7.5, 150 mM NaCl, 1 mM EDTA, 0.5% NP-40 in the presence of a protease inhibitor cocktail (Roche), 1 mM 1,10-phenantroline and 20 mM N-ethyl-maleimide to preserve Ub conjugates. DNA was cleared by the addition of benzoase (Novagen). The supernatant was cleared by centrifugation, and lysates were quantified using a BioRad Protein Assay by measuring absorbance at 595 nm.

**SUPPLEMENTAL REFERENCES**


Adams, P.D., Afonine, P.V., Bunkoczi, G., Chen, V.B., Davis, I.W., Echols, N., Headd, J.J., Hung, L.W., Kapral, G.J., Grosse-Kunstleve, R.W., *et al.* (2010). PHENIX: a comprehensive Python-based system for macromolecular structure solution. Acta Crystallogr D Biol Crystallogr *66*, 213-221.

Bekes, M., Rut, W., Kasperkiewicz, P., Mulder, M.P., Ovaa, H., Drag, M., Lima, C.D., and Huang, T.T. (2015). SARS hCoV papain-like protease is a unique Lys48 linkage-specific di-distributive deubiquitinating enzyme. Biochem J *468*, 215-226.

Cer, R.Z., Mudunuri, U., Stephens, R., and Lebeda, F.J. (2009). IC50-to-Ki: a web-based tool for converting IC50 to Ki values for inhibitors of enzyme activity and ligand binding. Nucleic Acids Res *37*, W441-445.

Chen, V.B., Arendall, W.B., 3rd, Headd, J.J., Keedy, D.A., Immormino, R.M., Kapral, G.J., Murray, L.W., Richardson, J.S., and Richardson, D.C. (2010). MolProbity: all-atom structure validation for macromolecular crystallography. Acta Crystallogr D Biol Crystallogr *66*, 12-21.

Cook, W.J., Jeffrey, L.C., Carson, M., Chen, Z., and Pickart, C.M. (1992). Structure of a diubiquitin conjugate and a model for interaction with ubiquitin conjugating enzyme (E2). J Biol Chem *267*, 16467-16471.

El Oualid, F., Merkx, R., Ekkebus, R., Hameed, D.S., Smit, J.J., de Jong, A., Hilkmann, H., Sixma, T.K., and Ovaa, H. (2010). Chemical synthesis of ubiquitin, ubiquitin-based probes, and diubiquitin. Angew Chem Int Ed Engl *49*, 10149-10153.

Emsley, P., Lohkamp, B., Scott, W.G., and Cowtan, K. (2010). Features and development of Coot. Acta Crystallogr D Biol Crystallogr *66*, 486-501.

Flierman, D., van der Heden van Noort, G.J., Ekkebus, R., Geurink, P.P., Mevissen, T.E., Hospenthal, M.K., Komander, D., and Ovaa, H. (2016). Non-hydrolyzable Diubiquitin Probes Reveal Linkage-Specific Reactivity of Deubiquitylating Enzymes Mediated by S2 Pockets. Cell Chem Biol *23*, 472-482.

McCoy, A.J., Grosse-Kunstleve, R.W., Adams, P.D., Winn, M.D., Storoni, L.C., and Read, R.J. (2007). Phaser crystallographic software. Journal of applied crystallography *40*, 658-674.

Merkx, R., de Bruin, G., Kruithof, A., van den Bergh, T., Snip, E., Lutz, M., El Oualid, F., and Ovaa, H. (2013). Scalable synthesis of gamma-thiolysine starting from lysine and a side by side comparison with delta-thiolysine in non-enzymatic ubiquitination. Chem Sci *4*, 4494-4498.

Otwinowski, Z.M., W. (1997). Methods in Enzymology (eds Carter, C. W. Jr. & Sweet, R. M.) *276*, 307-326.

Ratia, K., Kilianski, A., Baez-Santos, Y.M., Baker, S.C., and Mesecar, A. (2014). Structural Basis for the Ubiquitin-Linkage Specificity and deISGylating activity of SARS-CoV papain-like protease. PLoS pathogens *10*, e1004113.

Ratia, K., Saikatendu, K.S., Santarsiero, B.D., Barretto, N., Baker, S.C., Stevens, R.C., and Mesecar, A.D. (2006). Severe acute respiratory syndrome coronavirus papain-like protease: structure of a viral deubiquitinating enzyme. Proc Natl Acad Sci U S A *103*, 5717-5722.